Fan Noise Prediction System Development: Source/Radiation Field Coupling and Workstation Conversion for the Acoustic Radiation Code

H. D. Meyer
United Technologies Corporation
Hamilton Standard Division
Windsor Locks, Connecticut

April 1993

Prepared for
Lewis Research Center
Under Contract Number NAS3-25952

National Aeronautics and
Space Administration

FOREWORD

This report documents source/radiation field coupling and workstation conversion for computer codes that are part of a fan tone noise prediction system based on linearized acoustic theory for turbofan and Advanced Ducted Propeller (ADP) engines. The study was conducted as Task X under the Aero-Propulsion Technology (APT) program, NASA Contract NAS3-25952. The NASA Project Manager for this contract is Mr. M. Murray Bailey, and the NASA Task Manager for Task X is Dennis Huff, NASA Lewis Research Center. Dr. D. C. Mathews served as Task Manager for Pratt & Whitney.

TABLE OF CONTENTS

SECTION 1

INTRODUCTION

This document describes one portion of a fan noise prediction program designed to develop improved methodologies for source and noise field prediction. Other parts of the effort are described in separate reports. In particular, Reference 1 discusses improvements made to the Acoustic Radiation Code (herein referred to as the ARC), a finite element program for predicting noise radiation from a turbofan engine inlet. In Reference 2, evaluation of the ARC versus test data is described, along with work to update the wake model in the Bolt, Beranek and Newman/Pratt and Whitney Code (herein called the BBN/PWC). The BBN/PWC is a turbofan source noise code that was used to supply source input information to the ARC. Reference 3 presents work on a two-dimensional coupled cascade code that couples radiation between rotor and stator blade rows, while including swirl flow in the source region. Each of these efforts is aimed toward eventually obtaining better noise prediction tools for turbofan engines. The regions treated by the three codes are shown in Figure 1.

This report concentrates on three areas: providing information so that developers of internal aerodynamics or aeroacoustic codes can understand the input requirements for the ARC, and also, the specific input formulation needed so that the BBN/PWC can be used as a source; development of a coupled interface between the source and radiation models; and modifications to the ARC for use on the Sun™ and Silicon Graphics Iris™ UNIX™ workstations in use at Hamilton Standard, Pratt and Whitney, and NASA-Lewis.

The reason for the first and last areas was to bring on board a versatile tool for studying noise. The ARC was a desirable choice because of its prior record of good correlation with test data and because its use of wave envelope elements reduces computational requirements. Since numerous source codes can be used to drive the ARC, general information is provided about the interface; however, since the BBN/PWC, in particular, is used as a source in work here and in Reference 2, more specific information is needed regarding its interfacing. The code conversion portion is discussed in the appendix.

These efforts establish a noise prediction capability that progresses from the source region and then into the far field. Thus both the BBN/PWC and ARC regions shown in Figure 1 are now included in the predictions. The interface between the two regions is called the "fan face," in Reference 1, although the user may place this interface anywhere in the inlet. Hereafter, this cross section will be referred to as the "source input boundary."

The second area to be discussed is the coupling between the source and radiation regions. Work on it had its genesis in a desire to explore the possibility of obtaining more accurate predictions by feeding reflections back from the ARC to the source code. This work involved study of the waves reflected between the inlet back into the source region as well as development of a preliminary coupled code. This study was conducted in order to determine whether the contribution from the waves was sufficient to warrant the extra complexity of a coupled analysis. Related to this, there has been earlier work dealing with wave propagation and reflection in ducts (see refs. 4-8). This has been mainly analytical, providing reflection coefficients, but not indicating the effect on the source. The present work couples the ARC and BBN/PWC to obtain actual noise levels.

SUMMARY

The Acoustic Radiation Code (ARC) is a finite element program used on the IBM™ mainframe to predict far-field acoustic radiation from a turbofan engine inlet. In this report, requirements for developers of internal aerodynamic codes regarding use of their program output as input for the ARC are discussed. More specifically, the particular input needed from the Bolt, Beranek and Newman/Pratt and Whitney (turbofan source noise generation) Code (BBN/PWC) is described. In a separate analysis, a method of coupling the source and radiation models, that recognizes waves crossing the interface in both directions, has been derived. A preliminary version of the coupled code has been developed and used for initial evaluation of coupling issues. Results thus far have shown that reflection from the inlet is sufficient to indicate that full coupling of the source and radiation fields is needed for accurate noise predictions. Also, for this contract, the ARC has been modified for use on the Sun™ and Silicon Graphics Iris™ UNIX™ workstations. Changes and additions involved in this effort are described in an appendix.

SECTION 3

USING OUTPUT FROM SOURCE CODES IN THE ACOUSTIC RADIATION CODE

In order for the ARC to predict the noise in the far field, it needs input information from a fan source code. To see what information might be useful to developers and users of source codes in providing such input, a number of internal unsteady aerodynamic methods (Euler, potential, acoustic) were surveyed. Some already had codes associated with them, while others could lead to engine source noise predictors in the future. These included work of Adamczyk, Mulac, and Celestina (ref. 14); Chi (ref. 15); Ni (ref. 16); Verdon, Barnett, Hall, and Ayer (ref. 17); and others. It was seen that output from source prediction methods must be processed or designed to be in the particular form required by the ARC. Therefore, general information is provided in the subsection below that should help developers of internal aerodynamic and acoustics codes understand the input requirements for the ARC. Additionally, because the BBN/PWC was used as a source for source/far-field coupling work at Hamilton Standard (see next section) and for code evaluation and noise prediction efforts at Pratt and Whitney (ref. 2), a specific procedure was needed for its input to the ARC. This information is presented in a second subsection.

General Input Requirements

The ARC requires source definition at an arbitrary plane in the inlet, the "source input boundary." At this location, the pressure is considered to be the sum of a forward-going wave, P^+, and a backward-going wave, P^-. As mentioned previously, the user inputs mode information from P^+ and the ARC computes the radiation and the radial mode amplitudes for P^-. The information provided here shows more explicitly what is required. Observe that, for later reference, both the forward- and backward-going waves are included in the discussion. However, only the forward-going wave is needed to provide input for the ARC. Note that not all source codes have pressure available explicitly and some may be two- rather than three-dimensional. It is the burden of the user to process the codes so that information can be extracted in the form required for the ARC.

The full expression for the complex, nondimensional pressure, P, at the "source input boundary," is given by

$$P(r,\phi,t) = P^+(r,\phi,t) + P^-(r,\phi,t) = \sum_{s=-\infty}^{\infty} \sum_{n=1}^{N} \sum_{k=-\infty}^{\infty} [P^+_{mns} \Psi_m(\kappa_{mn} r) \exp\{i(m\phi - \gamma^+_{mns} x_o - sB\Omega t)\} + P^-_{mns} \Psi_m(\kappa_{mn} r) \exp\{i(m\phi - \gamma^-_{mns} x_o - sB\Omega t)\}] \quad (3.1)$$

where the circumferential mode index, m, must satisfy the condition $m = sB - kV$ (see the discussion regarding this in Section 4). In Equation 3.1, P is nondimensionalized using $\rho_\infty c_\infty^2$, where ρ_∞ and c_∞ are, respectively, reference values of the density and speed of sound. The cylindrical coordinates (r,ϕ,x) are shown in Figure 2. They are oriented as in the BBN/PWC. The quantity x_o is the axial coordinate value at the "source input boundary," n is the radial mode index, s is the harmonic of blade passage frequency, B the number of rotor blades, V the number of stator vanes, N the total

SECTION 2

BACKGROUND

This section gives a very brief sketch of the two codes that have been used in this work, the ARC and the BBN/PWC. Complete details regarding the former can be found in References 1, 9, and 10; details for the latter are in References 11, 12, and 13.

The ARC is a FORTRAN program used to study acoustic radiation from turbofan engines. It was developed at the University of Missouri-Rolla (UM-R) under the direction of Professor Walter Eversman. The code uses standard and wave-envelope type finite elements and an underlying potential mean flow to predict noise from axisymmetric ducts with or without centerbodies. Solutions calculated within the code are in terms of the velocity potential, $\Phi_m(x,r)$, associated with circumferential mode m, where the complete solution is $\Phi = \Phi_m(x,r) \exp\{i(\omega t - m\phi)\}$. Here x is the axial coordinate, r and ϕ are polar coordinates, ω is rotor radian frequency, and t is time. Acoustic pressures are computed from Φ_m. The program treats the ARC region indicated in Figure 1. As input, both the index m and the reduced frequency (equivalently, rotor rpm or tip speed) must be set, along with complex forward propagating radial mode pressure amplitudes at the "source input boundary." As mentioned in the previous section, the "source input boundary" is an arbitrary duct cross section where source information is input, and is the interface between source and radiation regions (see Figure 1). The ARC outputs complex backward propagating radial mode amplitudes at this same boundary. It also provides predictions for acoustic potential, pressure directivity, and acoustic pressure in the upstream radiation region.

The BBN/PWC is a FORTRAN program that calculates the sound produced by the interaction of stator vanes with the mean velocity deficit wakes generated by the rotor blades of a turbofan engine. The wakes produce unsteady loading on the vanes, and this loading then serves as the source for the sound. The BBN/PWC was developed originally by Bolt, Beranek and Newman. Later, improvements were added by Pratt and Whitney. The fan/stator geometry for this study is shown in Figure 2. The code predicts the amplitudes of both upstream and downstream propagating modes, along with their sound power, in an infinite annular duct. To accomplish this, it uses the standard Green's function approach. In this approach, the Green's function is expressed as an expansion of normal duct modes; the loading (i.e., pressure distribution) exerted by the vanes on the fluid is evaluated for use in the Green's function integral that gives the pressure anywhere in the duct. Knowledge of the upwash, i.e., the component of the wake velocity normal to the surface of the stator vanes, allows calculation of the pressure distribution on the vanes. This is done by dividing the stators into chordwise "strips" and computing the load on each "strip" assuming the stators to be a linear cascade of flat plates. By means of this process, once the upwash is known, the upstream and downstream pressure mode amplitudes are obtained in straightforward fashion.

where

$$\Gamma_2 = \int_{r_H}^{r_D} \Psi_m^2(\kappa_{mn} r)\, r dr \tag{3.7}$$

The coefficients $\bar{P}^-_{mns}$ are not of concern to the user, as they are determined by the ARC as part of the solution. (Actually, it is the related velocity potential that is computed.)

Using BBN/PWC Output

When the BBN/PWC is used to generate the complex modal amplitudes, a straightforward conversion formula gives the modal information, $\bar{P}^+_{mns}$, to be used by the ARC. This is obtained by noting that, for a given circumferential mode order m, the output pressure $\bar{P}^+_{ms}$, from the BBN/PWC, for a forward propagating wave at the "source input boundary," is given by

$$\frac{\bar{P}^+_{ms}}{\frac{1}{2}\rho_o U^2} = \sum_{n=1}^{N} A_{mns}\left[A_{mn} * J_m(\kappa_{mn} r) + B_{mn} * Y_m(\kappa_{mn} r)\right] \tag{3.8}$$

Observe that $\bar{P}^+_{ms}$, unlike P^+_{ms} in Equation 3.5, is dimensional; m and s denote the m^{th} circumferential mode and the s^{th} harmonic of blade passage frequency. In the above equation, ρ_o is the nominal flow density and U is the mean axial fluid velocity. The square-bracketed terms represent expressions for the normal mode functions. They are the same as the Ψ_m in Equation 3.1 except for the difference in the normalization for these between the BBN/PWC and the ARC. The coefficients A_{mns}, A_{mn}, and B_{mn} are quantities that can be extracted from the BBN/PWC during a run. The values A_{mns} are the upstream complex mode amplitudes, and the A_{mn} and B_{mn} are the weighting constants for the normalized mode shapes. Note that for the BBN/PWC, the output that is used here is defined at the leading edge of the stator blade row.

If one rewrites Equation 3.8 as

$$\frac{\bar{P}^+_{ms}}{\frac{1}{2}\rho_o U^2} = \sum_{n=1}^{N} A_{mns}\,\Psi_{mnx}\left[\frac{1}{\Psi_{mnx}}\{A_{mn} * J_m(\kappa_{mn} r) + B_{mn} * Y_m(\kappa_{mn} r)\}\right] \tag{3.9}$$

then the eigenmode in the square brackets is now normalized so that it has a maximum value of one. This is the same as for the ARC. The quantity Ψ_{mnx} is the maximum value of the eigenmode over the range $r_H \le r \le r_D$.

For the ARC, the forward-propagating wave portion of Equation 3.5 can be rewritten as

$$P^+_{ms} = \frac{\bar{P}^+_{ms}}{\rho_\infty c_\infty^2} = \sum_n \bar{P}^+_{mns}\left[\Gamma_2\{J_m(\kappa_{mn} r) - \frac{J'_m(\kappa_{mn})}{Y'_m(\kappa_{mn})} Y_m(\kappa_{mn} r)\}\right] \tag{3.10}$$

number of positive radial modes, Ω the rotor rotation rate, and t the time. The coefficients P^+_{mns} and P^-_{mns} are the complex pressure amplitudes for the modes and are nondimensionalized in the same manner as P.

Further, the functions Ψ_m are the duct eigenmodes and are given by

$$\Psi_m(\kappa_{mn}r) = \Gamma_1 \left\{ J_m(\kappa_{mn}r) - \frac{J'_m(\kappa_{mn})}{Y'_m(\kappa_{mn})} Y_m(\kappa_{mn}r) \right\} \tag{3.2}$$

where J_m and Y_m are the standard Bessel functions of first and second kind of order m, κ_{mn} is the eigenvalue for mode (m,n), and J'_m and Y'_m are the derivatives of J_m and Y_m. The quantity Γ_1 is a normalization constant chosen so that the maximum value of $\Psi_m(r)$ over the range $r_H \le r \le r_D$ is one. Here r_D is the duct outer radius and r_H is the hub radius. The parameters γ^+_{mns} and γ^-_{mns} are the forward-propagating and backward-propagating axial wave numbers for the $(m,n)^{th}$ mode and s^{th} harmonic of blade passage frequency. They are given by

$$\gamma^{\pm}_{mns} = \frac{1}{1-M^2} \left[\frac{MsB\Omega}{c_o} \pm \sqrt{\left[\frac{sB\Omega}{c_o}\right]^2 - (1-M^2)\kappa^2_{mn}} \right] \tag{3.3}$$

where M is the inlet axial flow Mach number and c_o is the speed of sound in the duct.

One can extract $P_{ms}(r)$, the complex amplitude of the $(m,s)^{th}$ harmonic of $P(r,\phi,t)$ with respect to r and t, by using the formula

$$P_{ms}(r) = \frac{B\Omega}{(2\pi)^2} \int_0^{\frac{2\pi}{B\Omega}} \int_0^{2\pi} P(r,\phi,t) \exp\{-i(m\phi - sB\Omega t)\} \, d\phi dt \tag{3.4}$$

Once this is done, P_{ms} has the form

$$P_{ms}(r) = P^+_{ms}(r) + P^-_{ms}(r) = \sum_{n=1}^{N} [\bar{P}^+_{mns}\Psi_m(\kappa_{mn}r) + \bar{P}^-_{mns}\Psi_m(\kappa_{mn}r)] \tag{3.5}$$

To drive the ARC with output from a source code not already written in modal form, the complex modal amplitude coefficients $\bar{P}^+_{mns}$ must be found from $P^+_{ms}(r)$ by Fourier inversion. To accomplish this inversion, the user must first have separated out the forward-going portion, $P^+_{ms}(r)$, of $P_{ms}(r)$, using an approach appropriate for his code. Then the inversion formula is

$$\bar{P}^+_{mns} = \frac{1}{\Gamma_2} \int_{r_a}^{r_b} P^+_{ms}(r)\Psi_m(\kappa_{mn}r)\, rdr \tag{3.6}$$

SECTION 4

DEVELOPMENT OF A COUPLED INTERFACE BETWEEN THE SOURCE AND RADIATION MODELS

There are two approaches used in this report for linking source codes to the ARC. The first and simplest way is to input forward wave information directly from a source code to the ARC. This involves just one pass of each code and was the approach used at Pratt and Whitney for code evaluation (ref. 2). In this process, the ARC solution provides reflected wave information at the interface between the two codes, but the effect of the reflections on the source is ignored. This is the approach that was just described in the previous section. When the reflections are small, this approach should be satisfactory.

Note that these reflected waves are the accumulated effect of reflection in the duct from the "source input boundary" to the inlet. From the mathematics, it is known that reflections will occur at any point in the duct where there are changes in geometry. These reflections have been studied in the past (see, for instance, refs. 4-8), but this report is believed to be the first to address the effects of the reflections on the source strength, i.e., blade loading.

When reflections are large, a more sophisticated method might be preferable, one that would recognize waves passing the interface in both directions. This approach would iterate between source and radiation codes and, it is hoped, improve accuracy in both regions.

As a first evaluation of reflection, the ARC alone was used. Reflections at the "source input boundary," due to unit modal inputs, were studied for a range of rotor tip speeds. Results from this investigation, described in the following subsection, demonstrated reflection large enough to justify proceeding further.

A preliminary coupled code version was then developed by modifying the BBN/PWC to accept reflected waves and generate updated stator loading. The implementation of this approach is sketched out in the second subsection. Then the results of an initial set of exploratory runs, showing the effect of coupling on both the source and far-field regions, are presented in a last subsection.

Reflection Ratio Curves

Using only the ARC, curves of reflection ratios, $|\,p^-/p^+\,|$, versus engine tip speed, V_T, were derived (see Figures 3 through 6). Here, p^- and p^+ are the reflected and incident complex pressure amplitudes, $\bar{P}^-_{mn}$ and $\bar{P}^+_{mn}$, at the "source input boundary." A unit modal amplitude was input for each choice of mode, (m,n), over a range of tip speeds. Reflected wave amplitudes for the first nine radial modes, for a given m, were obtained as output.

Runs were for the fan inlet described by the finite element mesh in Figure 7, which is the figure used later to illustrate the quality of PostScript output. Dimensions shown are based on a unit fan tip radius. The model is for one of the test cases used by the UM-R in the past to test out ARC

if the normal mode functions, Ψ_m, are written out as in Equation 3.2.

By setting $\bar{P}^+_{ms}$ in Equation 3.9 equal to $\bar{P}^+_{ms}$ in Equation 3.10, noting that the square-bracketed terms for each are equivalent, and equating coefficients of the bracketed terms because they are linearly independent functions, it follows that

$$\frac{\rho_o U^2}{2} A_{mns} \Psi_{max} = \rho_\infty c_\infty^2 \bar{P}^+_{mns} \tag{3.11}$$

From this, the conversion relation becomes

$$\bar{P}^+_{mns} = \frac{(\rho_o U^2/2) \Psi_{max} A_{mns}}{\rho_\infty c_\infty^2} \tag{3.12}$$

or, using ARC and BBN/PWC program variables

$$ZAI(n) = \frac{(MODIM)(PSIMAX)(AMNS)}{(RHOFS)(CFS)^2} \tag{3.13}$$

where *ZAI(n)* is $\bar{P}^+_{mns}$, *RHOFS* is ρ_∞, and *CFS* is c_∞ in the ARC; *MODIM* is $\rho_o U^2/2$, *PSIMAX* is Ψ_{max}, and *AMNS* is A_{mns} in the BBN/PWC. The numerator of Equation 3.13 is programmed into the BBN/PWC to output complex radial mode amplitudes in lb/in^2 (see ref. 2). This output can then be nondimensionalized using the denominator of Equation 3.13 to obtain ARC input. This input information is supplied to the ARC via Input Card 4 of the ARC module PRATRADH. (See the appendix for a discussion of ARC modules.)

Note that for coupling work at Hamilton Standard and for code evaluation work at Pratt and Whitney, the right-hand side of Equation 3.13 was multiplied by 10,000 so that accuracy would not be lost in the ARC during calculations. Afterwards, outputs were scaled back by 0.0001 to produce actual values.

Table 1
SCATTERING RATIOS FOR UNIT INPUT OF MODE (34,2) INTO (34,n)

n \ V_T	1,039	1,069	1,098	1,106	1,113	1,128	1,187	1,247
1	.047	.059	.159	.335	.373	.264	.136	.160
2	.087	.196	1.507	1.991	1.620	.750	.149	.111
3	.011	.012	.042	.046	.050	.038	.117	.439
4	.001	.005	.001	.003	.004	.004	.011	.020
5	.001	.007	.001	.002	.003	.002	.002	.007
6	.001	.001	.002	.003	.003	.002	.002	.003
7	.000	.000	.001	.001	.001	.001	.000	.001
8	.001	.001	.001	.002	.002	.001	.001	.002
9	.001	.001	.002	.003	.003	.002	.001	.001

n=2 cuton (1,088 ft/sec)

n=3 cuton (1,209 ft/sec)

Table 2
SCATTERING RATIOS FOR UNIT INPUT OF MODE (34,4) INTO (34,n)

n \ V_T	1,187	1,247	1,306	1,336	1,365	1,425
1	.007	.017	.023	.301	.104	.053
2	.011	.014	.018	.230	.068	.045
3	.062	.164	.039	.241	.059	.058
4	.036	.073	.302	3.906	.420	.088
5	.019	.027	.033	.322	.136	.477
6	.003	.003	.004	.038	.017	.054
7	.002	.002	.001	.004	.002	.004
8	.003	.002	.002	.013	.003	.003
9	.001	.001	.001	.007	.002	.001

n=3 cuton (1,209 ft/sec)

n=4 cuton (1,318 ft/sec)

n=5 cuton (1,420 ft/sec)

development. All results were for an inlet Mach number, M, of 0.5, a free stream Mach number of 0.3, and a 38-blade ($B = 38$) rotor.

Figure 3 shows reflection ratios vs. V_T for a fixed circumferential mode number of $m = 25$ and radial mode numbers of $n = 1$ to 4. Note that the peak of each curve occurs just a bit after the cut on tip speed of the corresponding mode. Reflection was considered to be important in regions where reflection ratios were 0.5 or greater. The horizontal bands in Figure 3 point out these regions. To quantify the widths of these bands, a bandwidth, W, was defined as

$$W = \frac{\Delta V_T(at\ |p^-/p^+| = .5)}{(midband\ V_T)} \times 100\%$$

for each curve. In this expression, ΔV_T (at $|p^-/p^+| = .5$) is the change in V_T in passing from the left to the right side of the curves at a height of 0.5. As seen from Figure 3, these bandwidths vary from 21% to 4%, where the bandwidth is greatest for $n = 1$. It can be seen that these bands cover more than half the speed range evaluated. We have looked at other m's and found similar behavior (see Figures 4 and 5). The curves in Figure 6 show the same point as above but for the situation where m varies and $n = 1$ is fixed. These curves, just as the previous ones, show that there is significant reflection in bands about cuton. Thus, Figures 3 through 6 show that there can be considerable reflection across the range of tip speeds important to turbofan engines.

One might question points on the curves in Figures 3 through 6 where the ratios were greater than one. However, note that higher pressures in the reflected waves do not imply higher acoustic powers. Numerical experiments with a two-dimensional analysis indicate that, at $M = 0.5$, unit reflection of power produced roughly a factor of 2.5 for $|p^-/p^+|$.

Figures 3 through 6 deal only with reflection from a fixed radial mode n to n. There is also reflection from one radial mode to another. This is addressed in Tables 1 and 2 below. Data is from the same series of runs that produced Figures 3 to 6, and is for the case where $m = 34$. The entries in the tables are the ratios $|p^-/p^+|$, where $|p^-|$ now represents the reflected pressure coefficient for each of the nine radial modes indicated. The input, p^+, for Table 1, is a unit amplitude for a relatively low order mode (34,2). For Table 2, the input is a unit amplitude for a slightly higher order mode (34,4). As can be seen from the data, there is scattering into both higher and lower order modes relative to the input mode. From the data in the tables, it is seen that there can be considerable reflection activity resulting from one radial mode reflecting into another.

Observe that a stairstep type line has been added to both of the tables to indicate the division between modes that are cut on and cut off. Looking at ratios adjacent to these boundaries, note the tendency for the strongest reflected mode to move along these lines. This observation is based on only a small amount of data, so it is something we would wish to look into further in the future.

It can be shown that the upwash has the form (see ref. 11, Equation 82)

$$w^{w} = \sum_{s} w_s \exp\left\{ik_s z + \frac{i2\pi vsB}{V} - isB\Omega t\right\} \tag{4.2}$$

relative to stator vane v, $v = 0, 1, \ldots, V-1$, where s, B, V, and Ω are the same as before. In Equation 4.2, an i has been added to the second term in the exponential; this was missing from Equation 82 of Reference 11. The w_s's are the Fourier coefficients of the wake upwash at the s^{th} harmonic of blade passage frequency, k_s is the chordwise wave number, and z is the local coordinate along each of the stator vanes. The expressions for w_s and k_s are the same as in Reference 11 except for differences produced by correcting for sign errors, by using the relative flow angle into the stator in place of the rotor stagger angle, and by shifting the z-origin from where the stator mid-chord meets the hub to where its leading edge intersects the hub. These modifications are needed to provide correspondence with the actual code.

Using Equation 4.2, an expression can be obtained for $\Delta\bar{p}_v$, which is the s^{th} harmonic of the pressure loading Δp appearing in Equation 4.1. It acts on vane v and (see ref. 11, Equation 86) is given by

$$\Delta\bar{p}_v = \rho_o U_r w_s f_s(r,z) \exp\{-i\,2\pi vsB/V\} \tag{4.3}$$

where ρ_o is the nominal fluid density and U_r is the fluid velocity relative to the stator vanes. The minus sign in the exponential corrects a sign error in Reference 11. The quantity $f_s(r,z)$ is the elemental stator vane loading function which comes from solving

$$\exp\{ik_s z\} = \int_0^{2b} K_c(z-y) f_s(r,z)\,\frac{dy}{b} \tag{4.4}$$

Here $K_c(z\text{-}y)$ is the kernel function for a linear cascade and is discussed in Reference 11, Appendix B. The integration is from 0 to $2b$, rather than from $-b$ to b as in Reference 11, because of the shift in origin for z mentioned previously.

By next returning to Equation 4.1, expanding G there in terms of eigenmodes, and then using Fourier transform relations, one can obtain an expression for the complex pressure modal amplitudes, p^{w}_{mns}. This expression will depend on $\Delta\bar{p}_v$ above. Using Equation 4.3 in this expression, one then obtains the relation (see ref. 11, Equation 187)

$$\frac{p^{w}_{mns}}{\tfrac{1}{2}\rho_o U^2} = \frac{\sigma_c (U_r/U)^2 V}{\pi(1-\sigma_r^2)\,\hat{k}_{mns}} \int_{\sigma_r}^{1} \left[\frac{w_s}{U_r}\right] \Psi_m(X_{mn}\sigma)\left(\frac{m}{\sigma}\cos\alpha_s + \bar{\gamma}_{mns}\sin\alpha_s\right) * \exp\left\{-i\left[\bar{\gamma}_{mns}\bar{\delta}_1 - \frac{m}{\sigma}\bar{\delta}_2\right]\sigma_c\right\} \bar{b} C_{mns}(\sigma)\,d\sigma \tag{4.5}$$

for the amplitudes, p^{w}_{mns}, nondimensionalized by $\tfrac{1}{2}\rho_o U^2$. The subscripts m, n, and s signify the

As a final note, observe that the shape of the curves in Figures 3 through 6 can be explained as follows. An input wave can be shown to propagate axially with complex amplitude proportional to the term $\exp\left\{-iA_1V_T x - A_2\sqrt{V_{T,CO}^2 - V_T^2}\,x\right\}$. Here A_1 and A_2 are positive constants, $V_{T,CO}$ is cut on tip speed, and x is the duct axial coordinate. This expression comes from rewriting the factor $\exp\{-i\,\gamma_{mns}^{+}x_o\}$ in Equation 3.1; x_o was generalized here to x and γ_{mns}^{+} was rewritten in terms of V_T and $V_{T,CO}$. Just below cuton, the $\left\{-A_2\sqrt{V_{T,CO}^2 - V_T^2}\,x\right\}$ portion of this exponential is real and nearly one. Hence, one would expect the input wave to propagate through the duct, from the "source input boundary" to the inlet, nearly undiminished, and one would expect the reflected wave to be largest in this tip speed region. Because this exponential decreased rapidly for V_T just a bit below cuton, the drop-off to the left of $V_{T,CO}$ should be steep, which it is.

To the right of $V_{T,CO}$, the square root part of the exponential becomes imaginary. Thus the whole exponential is sinusoidal and the input wave propagates toward the inlet undiminished. However, as V_T increases, the axial wavelength that is proportional to $1 / \left(A_1V_T + A_2\sqrt{V_T^2 - V_{T,CO}^2}\right)$ decreases relative to the annular width of the duct. As the wavelength decreases, more of the input wave will be radiated outside the inlet and less will be reflected. Hence the ratio, $|\,p^-/p^+\,|$ will drop off to the right of $V_{T,CO}$, as is seen in the curves.

Implementation of Coupling

To implement coupling, the source code was modified to make use of the reflected wave information from the ARC to update loading on the stator vanes and, from this, the modal amplitudes. The source code chosen for this purpose was the BBN/PWC. Because it was being used at Pratt and Whitney, it could be quickly brought on board; also, because it was based on the use of duct modes, as is the ARC, the mathematics for coupling was highly compatible. Before briefly describing how this was done, the approach used for the original derivation will be summarized here. The reader is referred to Reference 11 for further background. Note that the coupling implemented here is used for the runs described in the next subsection. These runs comprise the first step of an iteration process and are explored to establish the importance of coupling.

As mentioned in Section 2, the original BBN/PWC predicts the amplitudes, p_{mns}^{w}, of the pressure modes that are generated by the loading on the stator blades coming from the upwash, w^{w}, of the rotor wake. One starts with the Green's function representation for pressure (see ref. 11, Equation 4.1), which is given by

$$p(x,t) = -\int_{-\infty}^{\infty}\int_{S} n(y)\cdot\nabla G(x,y,t-\tau)\,\Delta p\,(y,\tau)\,dS(y)\,d\tau \qquad (4.1)$$

where S is the stator vane surface area, x and y are coordinate vectors (in cylindrical coordinates) in the duct, n is the unit normal to the stator blades, G is the Green's function, ∇ is the gradient operator, t and τ are time, and Δp is the pressure loading on the vanes.

The velocity, v^R, calculated from Φ^R_{ms}, is given by $v^R = \nabla \Phi^R_{ms}(r,\phi,x)$. This gives an expression for the velocity anywhere in the duct. If the component of v^R normal to the stator vanes is evaluated along the stator vanes, one has w^R. After proceeding through this calculation, coordinates and variables must be converted to those used in the BBN/PWC so that results can be used in this code. In doing this, differences in coordinate orientation, scaling, and definition of similar variables must be taken into consideration. Also, correct phasing must be maintained. The result is the relation

$$w^R = \sum_{j=1}^{N} w_{js} \exp\left\{ik_{js}z - i\frac{2\pi vsB}{V} - isB\Omega t\right\} \tag{4.9}$$

for the upwash, due to reflected waves, on vane v, $v = 0, 1, \ldots, V-1$.

In Equation 4.9, the w_{js}'s are the Fourier coefficients of the reflection upwash at the s^{th} harmonic of the blade passage frequency for radial mode j, and k_{js} is the chordwise wave number. The quantities w_{js} and k_{js} correspond to w_s and k_s in Equation 4.2, but the expressions defining these are obviously very different. The quantities above depend on r, α_s, $\bar{\Phi}_{mjs}$, $\bar{\gamma}_{mjs}$, and the vane sweep parameters.

If one proceeds from this point as previously for the wake case, one then obtains the pressure modal amplitudes, p^R_{mns}, representing the effect of reflections from the inlet striking the stator and re-radiating upstream. They are nondimensionalized by $\frac{1}{2}\rho_o U^2$ and are as given below:

$$\frac{p^R_{mns}}{\frac{1}{2}\rho_o U^2} = \frac{\sigma_c (U_r/U)^2 V}{\pi(1-\sigma_r^2)\hat{k}_{mns}} \sum_{j=1}^{N} \int_{\sigma_r}^{1} \left[\frac{w_{js}}{U_r}\right] \Psi_m(X_{mn}\sigma) * \left[\frac{m}{\sigma}\cos\alpha_s + \bar{\gamma}_{mjs}\sin\alpha_s\right] \bar{b}C_{jmns}(\sigma)\,d\sigma \tag{4.10}$$

Just as for the wake case, the mathematics that gives Equation 4.10 requires that m be such that $m = sB - kV$, where k may be any integer. The functions $C_{jmns}(\sigma)$ depend on, among other things, the geometry, wave numbers, and the elemental vane chordwise pressure distributions, $f_{js}(r,z)$. Analogous to the situation for the $f_s(r,z)$ in the wake case, the $f_{js}(r,z)$ are calculated by solving the integral equation

$$\exp\{ik_{js}z\} = \int_0^{2b} K_c(z-y) f_{js}(r,z)\frac{dy}{b} \tag{4.11}$$

where $K_c(z\text{-}y)$ is the kernel function employed before. Observe that there are no phase terms in Equation 4.10 similar to the one in Equation 4.5. This is because such terms have been absorbed into the w_{js}'s in Equation 4.10.

As a last comment, note that the modifications described above have been incorporated into the SRCHV, FILLOV, PRES, OPFILE, and CLFILE subroutines of the BBN/PWC.

$(m,n)^{th}$ mode at the s^{th} harmonic of blade passage frequency. In Equation 4.5, U is the axial fluid velocity; $\sigma_c = 2b_T/r_D$ where b_T is the vane semi-chord at the tip and r_D is the duct outer radius; $\sigma_r = r_H/r_D$ is the hub radius; and $\bar{\gamma}_{mns} = \gamma_{mns} r_D$ where γ_{mns}, the axial wave number, is the same as $\gamma^{\pm}_{mns}$ in Equation 3.3. In defining γ_{mns}, γ^{+}_{mns} or γ^{-}_{mns} is picked according to whether p^{W}_{mns} is for an upstream-going wave or for a downstream-going wave. Further, in Equation 4.5, $\bar{k}_{mns} = k_{mns} r_D$ where k_{mns} is the square root portion of γ_{mns}; Ψ_m is the normal mode; $X_{mn} = \kappa_{mn} r_{D_1}$ where κ_{mn} is the eigenvalue for mode (m,n); $\sigma = r/r_D$; α_s is the stator stagger angle; δ_1 and δ_2 are nondimensionalized vane sweeps; $\bar{b} = b/b_T$, where b is the vane semi-chord; and the C_{mns} are the chordwise functions appearing in Reference 11, but with minor modifications. Note that p^{W}_{mns} in Equation 4.5 is nondimensionalized using $\frac{1}{2}\rho_o U^2$, rather than $\rho_o U^2$ as in Reference 11, so that the expression corresponds to that in the code; also, typographical errors have been corrected. Lastly, observe that the mathematics to arrive at Equation 4.5 imposes the condition that $m = sB - kV$, where k may be any integer. The right-hand side is opposite in sign to the condition in Reference 11, because of an error there.

For the modified version of the BBN/PWC, an additional upwash, w^R, due to reflected waves, must be calculated. The noise is now produced by an upwash, w, on the stator, given by

$$w = w^W + w^R \tag{4.6}$$

The upwash w^W is the same as before; the additional upwash, w^R, is calculated using the reflected wave information provided by the ARC. Because each ARC run is for a fixed frequency, $\omega = sB\Omega$, w^R will not be given by a sum of terms over s as was w^W (see Equation 4.2), but will be given by only one such term. Once w^R is found, the pressure amplitude coefficients, p^R_{mns}, can be determined by a process parallel to that used above to derive the p^W_{mns}. Then the total pressure amplitude is

$$p_{mns} = p^W_{mns} + p^R_{mns} \tag{4.7}$$

To obtain w^R, one starts with the velocity potential for the reflected wave, which is given by

$$\Phi^R_{mns} = \sum_{j=1}^{N} \Phi^-_{mjs} \Psi_m(\kappa_{mj} r) \exp\{i(-m\phi - \gamma^-_{mjs} x + sB\Omega t)\} \tag{4.8}$$

The variables and coordinates here are those used by the ARC. This means that the orientation for (r,ϕ,x) and Ω is opposite to that shown in Figure 2, which gives the orientation used by the BBN/PWC. Variables have the scaling used by the ARC; the x-origin, the axial position where the "source boundary interface" is located, falls where the leading edge of the stator intersects the hub.

The subscripts m and s, on the left, are the indices assumed for the ARC run. The coefficients Φ^-_{mjs} are the velocity potential complex modal amplitudes from the solution for the reflected waves. There are N of these, corresponding to the number of positive radial modes, indexed by j, chosen for the ARC run. The modes can be cut on or cut off because both types are permitted by the ARC. However, the BBN/PWC only computes cut on modes. Hence, the loading generated by Equation 4.8 will only contribute to those radial modes, specified below by the index n, which are propagating modes in the BBN/PWC.

somewhat removed from cuton, the patterns are essentially the same but the levels are different. At the second tip speed, nearer to cuton, both the shapes and the amplitudes vary.

Current efforts show that coupling is important. However, present results are for only one iteration step. It will be important in future work to continue the iteration and study convergence.

Coupled Runs

The calculations presented in the first subsection showed there is considerable reflection activity in the duct. To further explore the importance of this, an initial study of the effect of coupling on noise levels was begun. To this end, a series of computer runs was made that coupled the BBN/PWC with the ARC. For a given tip speed (actually rpm in the BBN/PWC and reduced frequency in the ARC), each run involved first executing the BBN/PWC, then feeding its output as input to an initial ARC run. Reflected wave output from this ARC run, at the "source input boundary," was next fed into a second BBN/PWC run where it provided updated stator blade loading. The resulting BBN/PWC output was then used as input for a second ARC run.

These initial tests were made for the same geometry (see Figure 8) as used in the evaluation studies at Pratt and Whitney (ref. 2) for a similar tip speed range, 9,300-12,000 ft/sec. The setup treated a 16-blade, 22-vane, two-chord spacing, medium length ADP inlet model. The exterior Mach number was 0.2. The circumferential mode number studied was m = -6, also studied by Pratt and Whitney, and only the first BPF harmonic was used. Essentially the same input as used at Pratt and Whitney for the V_T = 788 ft/sec case was used as a starting point. The rest of the coupled runs employed the same properties, changing only the tip speeds. In the coupled BBN/PWC runs, the first nine radial modes for m = -6, not all of which were cut on, were used. This is permissible (see the discussion in the previous subsection) even though the BBN/PWC only gives output for cut on modes.

Results are shown in Figures 9 through 12. Figure 9 compares total upstream sound power in the first and second BBN/PWC runs, i.e., before and after coupling, as a function of tip speed. Note that cuton for the second radial mode, (-6,2), is at 706 ft/sec where the two curves peak. Below this speed only radial mode (-6,1) contributes to power; above this point both modes (-6,1) and (-6,2) contribute. Observe that radial modes (-6,1) and (-6,2) here correspond to (-6,0) and (-6,1) in Reference 2. It is seen that in a band of tip speeds above second radial mode cuton, there is a sizable increase in total power from the uncoupled to the coupled case. (Note that the increase just below cuton of the (-6,2) mode here and in Figure 10 should be disregarded; we trust that had there been additional points computed in this vicinity, there would have been virtually no delta.) At a typical point, V_T = 788 ft/sec, a bit removed from cuton, the increase is 5.7 dB.

Figure 10 shows a similar comparison for the ARC between the first and second runs, where the first is before coupling and the second is after. The ordinate here is maximum sound pressure level at 10 inlet radii, rather than total power as before. This quantity is used because it, rather than total power, is easily derivable from ARC runs. Also, it was felt that this parameter gave a good indication as to whether coupling was, or was not, having an effect. Just as for the prior BBN/PWC case, plots here show a band above cuton where the change in noise levels due to coupling is significant, and at V_T = 788 ft/sec, the increase in SPL was comparable to the power increase computed via the BBN/PWC.

Figures 11 and 12 illustrate further the effect of coupling on far-field noise. Figure 11 shows the change in pressure directivity patterns in passing from the first to the second ARC run at V_T = 788 ft/sec. Figure 12 gives the same information at V_T = 710 ft/sec, which is nearer to cuton. Both show that coupling has made a major difference in noise results. At the first tip speed,

SECTION 6

APPENDIX

CONVERSION OF THE ACOUSTIC RADIATION CODE TO THE WORKSTATION

This appendix discusses modifications that were made to the ARC so that it would run on Sun and Silicon Graphics Iris UNIX workstations. The changes were of two types. The first set consisted of those that were needed to bridge the gap between what was acceptable for the UNIX/FORTRAN workstation-based environment as opposed to the IBM mainframe one, which was more forgiving. The second, and main change, involved adding subroutines to provide the PostScript™ plot output requested by NASA. The original code provided CalComp™ output.

The workstation version consists of the five modules listed below. The designations for them are the same as for the UM-R modules except that an "H," for Hamilton Standard, has been added to the names of the workstation versions to distinguish between the two.

PRATREH - generates input data for nacelle and centerbody geometry for use in PRATMESHH

PRATMESHH - generates the finite element mesh and the duct eigenvalue solution

PRATFLOWH - obtains the potential flow solutions

PRATVELH - superposes the solutions above for use in PRATRADH

PRATRADH - generates the acoustic radiation solutions

Note that there are two UM-R modules, PRATRADA and PRATRADB, corresponding to the workstation version, PRATRADH. The first of these uses CalComp plot routines, while the second creates plot files for a commercial program called TECPLOT™. Because a non-proprietary approach was preferred, PRATRADA, rather than PRATRADB, was chosen for workstation conversion. Also note that the input and output descriptions for both the workstation and IBM mainframe versions of the above modules are the same. See Reference 1, Appendix A, for a description of the input and output for the modules.

IBM-to-UNIX Changes

This subsection discusses changes that were needed because some coding, though acceptable in the IBM mainframe environment, would not work in the Sun/Silicon Graphics one. Of the five modules above, PRATPREH remained essentially the same as the original. The other four required changes.

SECTION 5

CONCLUDING REMARKS

In this report, information was presented regarding use of output from source codes as input for the ARC (Acoustic Radiation Code). This involved describing general input requirements for any source code as well as for specific ones for the Bolt, Beranek and Newman/Pratt and Whitney Code (BBN/PWC). A result of this effort is a one-pass capability using both the BBN/PWC and the ARC to predict noise in both the source and far-field regions. Development of a coupled interface between the source and radiation models was described. In this regard, the BBN/PWC was modified to accept reflected wave input from the ARC. This input was used to update blade loading, by means of which noise predictions were updated. In the appendix which follows this section, conversion of the ARC from the University of Missouri-Rolla IBM mainframe version to the Sun and Silicon Graphics Iris UNIX workstation versions is discussed.

The coupling process and reflection in the duct were studied. Using the ARC alone, unit amplitude forward propagating modes were input at the "source input boundary." The code computed the reflected amplitudes for the same radial modes as those input. The ratio of these amplitudes, $| p^-/p^+ |$, versus rotor tip speed, for a selection of circumferential mode and radial mode pairs, (m,n), indicates that in significantly wide bands about cut on tip speed, there is significant reflection from the inlet. There was also significant reflection into other radial modes in the vicinity of cut on boundaries

Additional runs were made using the BBN/PWC-ARC preliminary coupled version of the code for an ADP model, with circumferential mode order m = -6. For this process, a first BBN/PWC run was made. Output from this first run was fed into the ARC. Then this BBN/PWC-ARC cycle was repeated. Plots of total sound power versus tip speed for propagating waves in the duct and of maximum sound pressure level versus tip speed for waves at 10 inlet radii in the far field, showed significant increases in radiation levels in a band above second radial mode cuton. For instance, at a tip speed of 788 ft/sec (cuton was at 706 ft/sec), the increase in total power in the duct was 5.7 dB; a similar increase in SPL was also seen in the far field.

Based on results thus far, we can conclude that coupling reflection back to the source does have an effect on net radiation and should be included in predictions. Note, however, that work here has been for only one iteration step. In the future, further iterations need to be studied and convergence should be investigated.

In view of the above remarks, there are a number of recommendations regarding further work in this area. Coupling should continue to be studied by further developing the code that links the ARC and the BBN/PWC. Changes in stator loading, sound pressure, or power in the source region and far field, and scattering between radial modes should be investigated further. By means of additional runs over a range of tip speeds of interest to ADP engines, additional light should be shed on physical, computational, and mathematical aspects of coupling. As part of this additional work, behavior close to additional cut off points should be studied and, as pointed out above, convergence issues should be considered.

The second difference does not involve code. The Silicon Graphics compiler interprets record lengths of unformatted direct access files as numbers of words rather than numbers of bytes, as for the Sun. Code could have been changed for the Silicon Graphics to account for this; however, to keep both versions as nearly the same as possible, this was not done. By using the "-old_rl" option during compilation, record lengths are interpreted as bytes rather than words, thus accomplishing the same end.

Adding PostScript Output Capability

Plotting in the original code was accomplished through calls to standard CalComp routines. To provide PostScript plots, instead, PostScript subroutines were written to take the place of the CalComp equivalents. These generate a plotting file, fort.14, for each of the modules, PRATMESHH, PRATFLOWH, PRATVELH, PRATRADH, that later can be plotted out on a PostScript plotter or viewed on a monitor by means of one of the utility programs available for the Sun or Silicon Graphics workstations. Examples of PostScript plots are shown in Figure 7.

The PostScript subroutines that were added are listed below. They have the same arguments and perform the same functions as the original CalComp subroutines.

SYMBOL (X, Y, HEIGHT, IBCD, ANGLE, NCHAR)
- prints text or special symbols

PLOT (X, Y, IPEN)
- moves pen, either up or down, in a straight line to a new location

PLOTS (I, J, K)
- initializes the PLOT subroutine

NUMBER (X, Y, HEIGHT, FPN, ANGLE, NDEC)
- prints a number

Arguments for the above subroutines are defined as follows:

X, Y - coordinates to which pen is moved or where symbol or number is placed

HEIGHT - height of character or number

IBCD - the text or integer to be printed

ANGLE - angle from the horizontal at which to print text or number

NCHAR - number of characters to be printed

The most changes were needed to correct difficulties with plotting. In this connection, some general changes related to maintaining consistent data-typing were required. These were to insure that particular variables were of the same data-type and precision, double or single, when used in different routines, and also to make sure that there were no conflicts between the arguments in the calling statements for subroutines and the argument definitions in the subroutines themselves.

In particular, "IMPLICIT REAL*8 (A-H, O-Z)" and "IMPLICIT INTEGER*4 (I-N)" declarations were added at the beginning of most routines and function subprograms. Also, all "REAL," "INTEGER," and "COMPLEX" data-type declarations for particular variables were standardized to be "REAL*8," "INTEGER*4," and "COMPLEX*16." Additionally, double-precision constants were written in exponential "D-notation" (e.g., 12.5D+0) in subroutine argument lists, function calls, and elsewhere.

Further adjustments were also needed to eliminate problems in plotting. In PRATFLOWH, PRATVELH, and PRATRADH, the subroutine CONTUR needed changes. The same was true for the subroutine CONTP in PRATRADH. Both of these subroutines assist in contour plotting and were causing nondesired coordinates to be defined and plotted together with intended ones when they called the subroutine NWPLT2. Note that NWPLT2 is used to plot different types of curves (solid, chain-dotted, and dotted). Difficulties were cleared up by changing "CALL NWPLT2 (XP, RP, 2, ITYPE, PLOTD)" to "CALL NWPLT2 (XP, RP, 3, ITYPE, PLOTD)" in CONTUR and CONTP, and changing the coordinates XP(2) and RP(2) to XP(3) and RP(3). "INPT=2" was changed to "INPT=3." In NWPLT2, the statement "NS=NP*IDBL" was modified to be "NS = NP"; NS was a limit index-value for a DO-LOOP where coordinates were defined. This latter change was also made in the subroutine NWSCLE which was used in all the ARC modules except PRATPREH; NWSCLE sets up suitable ranges for a given set of points when plotting. The purpose of this change was to be sure that coordinates were properly defined in NWSCLE also.

Regarding nonplotting-related changes, in the EIGEN subroutine of PRATMESHH, there was originally a call to the IBM mainframe service routine, XUFLOW. This suppresses interrupts to the program from exponent underflow, which could be disruptive. The call to XUFLOW was disabled in the workstation version because it is not available there. Nothing was added to replace this because default IEEE floating point exception handling for UNIX workstations does nearly the same thing as XUFLOW.

There were a number of other, generally minor, changes made to the code, even though they would have no immediate effect on workstation runs. The first of these was implemented with the thought of eliminating possible future difficulties should the code be moved, later, to other computer platforms. Most of these dealt with eliminating additional minor data-typing inconsistencies between calling programs and subroutines. These were suggested through tests using the Lahey™ FORTRAN compiler on the IBM PC™ and using the ICA (Intercompilation Analysis) option during IBM mainframe compilations.

Note that there are two slight differences between the Sun and Silicon Graphics versions of the program. The first regards coding where, for the Sun, in PRATRADH, an "OPEN (UNIT=6, FORM='PRINT')" statement was added to prevent unwanted control characters from being printed out in hardcopy. The option "PRINT" is not available for Silicon Graphics workstations.

SECTION 7

REFERENCES

1. Roy, D. R., Eversman, W., and Meyer, H. D., "Improved Finite Element Modeling of the Turbofan Engine Inlet Radiation Problem," April, 1993.

2. Topol, D. A. and Philbrick, D. A., "Fan Noise Prediction System Development: Wake Model Improvements and Code Evaluations," April, 1993.

3. Hanson, D. B., "Fan Noise Prediction System Development: Unsteady Coupled Cascade Theory Applied to the Rotor/Stator Interaction Noise Problem," NASA CR-4506, May, 1993.

4. Levine, H. and Schwinger, J., "On the Radiation of Sound from an Unflanged Circular Pipe," Physical Review, Vol. 73, No. 4, February, 1948, pp. 383-406.

5. Rice, E. J., "Multimodal Far-Field Acoustic Radiation Pattern Using Mode Cutoff Ratio," AIAA Journal, Vol. 16, No. 9, September, 1978, pp. 906-911.

6. Morfey, C. L., "Rotating Pressure Patterns in Ducts: Their Generation and Transmission," J. Sound and Vibration, Vol. 1, 1964, pp. 60-87.

7. Zorumski, W. E., "Generalized Radiation Impedances and Reflection Coefficients of Circular and Annular Ducts," J. Acoustical Society of America, Vol. 54, December, 1973,pp. 1667-1673.

8. Cho, Y. C., "Sound Radiation from Hyperboloidal Inlet Ducts," AIAA Paper No. 79-0677, presented at AIAA 5th Aeroacoustics Conference, March 12-14, 1979, Seattle, Washington.

9. Eversman, W., Parrett, A. V., Preisser, J. S., and Silcox, R. J., "Contributions to the Finite Element Solution of the Fan Noise Radiation Problem," Transactions of the ASME, Vol. 107, No. 2, April, 1985, pp. 216-223.

10. Parrett, A. V. and Eversman, W., "Wave Envelope and Finite Element Approximations for Turbofan Noise Radiation in Flight," AIAA Journal, Vol. 24, No. 5, May, 1986, pp. 753-760.

11. Ventres, C. S., Theobald, M. A., and Mark, W. D., "Turbofan Noise Generation, Volume 1: Analysis," NASA CR-167951, July, 1982.

12. Ventres, C. S., Theobald, M. A., and Mark, W. D., "Turbofan Noise Generation, Volume 2: Computer Programs," NASA CR-167952, July, 1982.

13. Topol, D. A., and Mathews, D. C., "Rotor Wake/Stator Interaction Noise Prediction Code," Technical Documentation and User's Manual, NASA Report, October, 1992.

IPEN	- 2 = pen down; 3 = pen up; -2 or -3 establishes new origin
I, J	- no longer used; set to 0
K	- logical output device number
FPN	- floating point number to be printed
NDEC	- controls precision of number printed

Further details regarding the functions and arguments of the above subroutines can be found in the CalComp manual (ref. 18).

Note that in transferring to PostScript from CalComp, it was necessary, also, to modify a very small amount of plotting-related code in some of the ARC modules. This was to adjust the spacing for text and numbers so that they would fall in the proper locations under PostScript. Keeping the original CalComp placement would not have done this.

SECTION 8

LIST OF SYMBOLS

b	vane semi-chord
$\bar{b}$	b/b_T
b_T	vane semi-chord at tip
c_o	speed of sound in duct
c_∞	ARC reference value for speed of sound
exp { }	exponential function
$f_s(r,z)$	elemental vane chordwise pressure distribution for s^{th} harmonic of blade passage frequency
$f_{js}(r,z)$	elemental vane chordwise pressure distribution for j^{th} radial mode and s^{th} harmonic of blade passage frequency
i	$\sqrt{-1}$
k_s	vane chordwise wave number for s^{th} harmonic of blade passage frequency
k_{js}	vane chordwise wave number for j^{th} radial mode and s^{th} harmonic of blade passage frequency
k_{mns}	square root portion of γ_{mns}
$\hat{k}_{mns}$	$k_{mns} r_D$
m	circumferential mode index
n	radial mode index
$\boldsymbol{n}$	unit vector in direction normal to stator vanes
p	acoustic pressure
p^-	complex amplitude for reflected pressure wave at "source input boundary"
p^+	complex amplitude for incident pressure wave at "source input boundary"

14. Adamczyk, J. J., Mulac, R. A., and Celestina, M. L., "A Model for Closing the Inviscid Form of the Average-Passage Equation System," ASME Paper No. 86-GT-227, June, 1986.

15. Chi, R. M., "Three-Dimensional Subsonic Unsteady Lifting Surface Theory for Ducted Fan," UTRC Report No. R90-255135-1, October, 1990.

16. Ni, R. H., "Flow Simulation in Multistage Turbine," presented at the NASA Marshall Space Flight Center Computational Fluid Dynamics Workshop, April, 1987.

17. Verdon, J. M., Barnett, M., Hall, K. C., and Ayer, T. C., "Development of Unsteady Aerodynamic Analyses for Turbomachinery Aeroelastic and Aeroacoustic Applications," NASA CR-4405, October, 1991.

18. California Computer Products, Inc. (CalComp), "Programming CalComp Electromechanical Plotters," December, 1977.

19. Woodward, R. P., Bock, L. A., Heidelberg, L. J., and Hall, D. G., "Far-Field Noise and Internal Modes from a Ducted Propeller at Simulated Aircraft Takeoff Conditions," AIAA Paper No. 92-0371, presented at AIAA 30th Aerospace Sciences Meeting & Exhibit, January 6-9, 1992, Reno, Nevada.

A_{mn}	first weighting constant used in BBN/PWC to normalize eigenmode (m,n)
AMNS	BBN/PWC program variable for nondimensional upstream pressure complex amplitude for mode (m,n) and s^{th} harmonic of blade passage frequency
A_{mns}	nondimensional upstream pressure complex amplitude for mode (m,n) and s^{th} harmonic of blade passage frequency in BBN/PWC
B	number of rotor blades
BMN	BBN/PWC program variable for second weighting constant used in normalizing eigenmode (m,n)
B_{mn}	second weighting constant used in BBN/PWC to normalize eigenmode (m,n)
CFS	ARC program variable for c_{mn}
$C_{mns}(\ )$	function used in Equation 4.5
$C_{jmns}(\ )$	function used in Equation 4.10
$G(\ )$	time-dependent Green's function for hard-walled annular duct
$J_m(\ )$	Bessel function of the first kind of order m
J_m'	first derivative of J_m
$K_c(\ )$	kernel function for linear cascade
M	inlet axial flow Mach number
MODIM	BBN/PWC program variable for $\rho_o U^2/2$
N	total number of positive radial modes for ARC run
$P(r,\phi,t)$	ARC complex nondimensional pressure at "source input boundary"
$P^-(r,\phi,t)$	complex nondimensional pressure for backward-propagating wave at "source input boundary"
$P^+(r,\phi,t)$	complex nondimensional pressure for forward-propagating wave at "source input boundary"

p_{mns}	$P^W_{mns} + p^R_{mns}$
p^R_{mns}	complex amplitude of acoustic pressure, produced by reflected waves, for mode (m,n) and s^{th} harmonic of blade passage frequency
p^W_{mns}	complex amplitude of acoustic pressure, produced by wake, for mode (m,n) and s^{th} harmonic of blade passage frequency
r	polar radius in cylindrical coordinates
r_D	duct outer radius
r_H	hub radius
s	index for harmonic of blade passage frequency
t	time
v	stator vane index number
v^R	velocity in duct produced by reflected waves
w	$w^W + w^R$
w_s	Fourier coefficient of wake upwash on stator vane for s^{th} harmonic of blade passage frequency
w^R	upwash along stator vanes produced by reflected waves
w^W	upwash along stator vanes produced by wake
w_{js}	Fourier coefficient of reflected wave upwash on stator vane for j^{th} radial mode and s^{th} harmonic of blade passage frequency
x	axial coordinate in cylindrical coordinates
x	field point for Green's function in cylindrical coordinates
x_o	axial coordinate value at the "source input boundary"
y	vane chordwise variable
y	integration point for Green's function in cylindrical coordinates
z	vane chordwise variable

$Y_m(\ )$	Bessel function of the second kind of order m
$Y_m'(\ )$	first derivative of $Y_m(\ )$
W	bandwidth for reflection ratio curves
$ZAI(n)$	complex amplitude for forward nondimensional pressure wave, with radial mode number n, at the "source input boundary"
α_s	vane stagger angle
γ_{mns}	axial wave number for $(m,n)^{th}$ mode and s^{th} harmonic of blade passage frequency
$\bar{\gamma}_{mns}$	$\gamma_{mns} r_D$
γ^-_{mns}	axial wave number for reflected wave for mode (m,n) and s^{th} harmonic of blade passage frequency
γ^+_{mns}	axial wave number of forward-propagating wave for mode (m,n) and s^{th} harmonic of blade passage frequency
Γ_1	normalization constant used in Equation 3.2
Γ_2	normalization constant defined in Equation 3.7
Δp	pressure loading on stator vanes in time domain
$\Delta\bar{p}_\nu$	pressure loading on stator vane ν in frequency domain
$\bar{\delta}_1, \bar{\delta}_2$	nondimensionalized stator vane sweeps
∇	gradient operator
κ_{mn}	eigenvalue for mode (m,n)
ρ_o	BBN/PWC nominal flow density
ρ_{ref}	ARC reference value for density
σ	r/r_D
σ_c	$2b_T/r_D$

$P_{ms}(r)$ complex nondimensional amplitude for $(m,s)^{th}$ harmonic of $P(r,\phi,t)$ with respect to r and t at "source input boundary

$P^{-}_{ms}(r)$ backward-propagating wave portion of $P_{ms}(r)$ at "source input boundary"

$P^{+}_{ms}(r)$ forward-propagating wave portion of $P_{ms}(r)$ at "source input boundary"

$\bar{P}^{+}_{ms}$ complex amplitude for $(m,s)^{th}$ harmonic of $P(r,\phi,t)$ with respect to r and t for forward-propagating wave at "source input boundary"

P^{-}_{mns} reflected wave complex nondimensional pressure amplitude for mode (m,n) and s^{th} harmonic of blade passage frequency, as used in Equation 3.1

P^{+}_{mns} complex nondimensional pressure amplitude for forward-propagating pressure wave for mode (m,n) and s^{th} harmonic of blade passage frequency, as used in Equation 3.1

$\bar{P}^{-}_{mns}$ complex nondimensional pressure amplitude for reflected wave for mode (m,n) and s^{th} harmonic of blade passage frequency, as used in Equation 3.5

$\bar{P}^{+}_{mns}$ complex nondimensional pressure amplitude for forward-propagating pressure wave for mode (m,n) and s^{th} harmonic of blade passage frequency, as used in Equation 3.5

PSIMAX BBN/PWC program variable for Ψ_{max}

RHOFS ARC program variable for ρ_{∞}

S stator vane surface area

U BBN/PWC mean axial fluid velocity

U_r fluid velocity relative to stator vanes

V number of stator vanes

V_T rotor tip speed

$V_{T,CO}$ rotor cut on tip speed

X_{mn} $\kappa_{mn} r_D$

ACKNOWLEDGEMENT

The author would like to thank D. B. Hanson for suggesting the project treated here and for his support and helpful suggestions.

σ_r	r_H/r_D
τ	time
ϕ	polar angle in cylindrical coordinates
Φ	ARC velocity potential, with space and time dependency
$\Phi_m(x,r)$	(x,r)-dependent portion of Φ
Φ^R_{ms}	ARC velocity potential, with space and time dependency, for reflected waves
$\bar{\Phi}_{mns}$	complex amplitude for ARC reflected wave velocity potential for mode (m,n) and s^{th} harmonic of blade passage frequency
$\Psi_m(\ )$	ARC normal duct mode for circumferential mode m
Ψ_{max}	maximum value of the duct eigenmode over the range $r_H \leq r \leq r_D$ for BBN/PWC
ω	radian frequency
Ω	rotor rotation rate

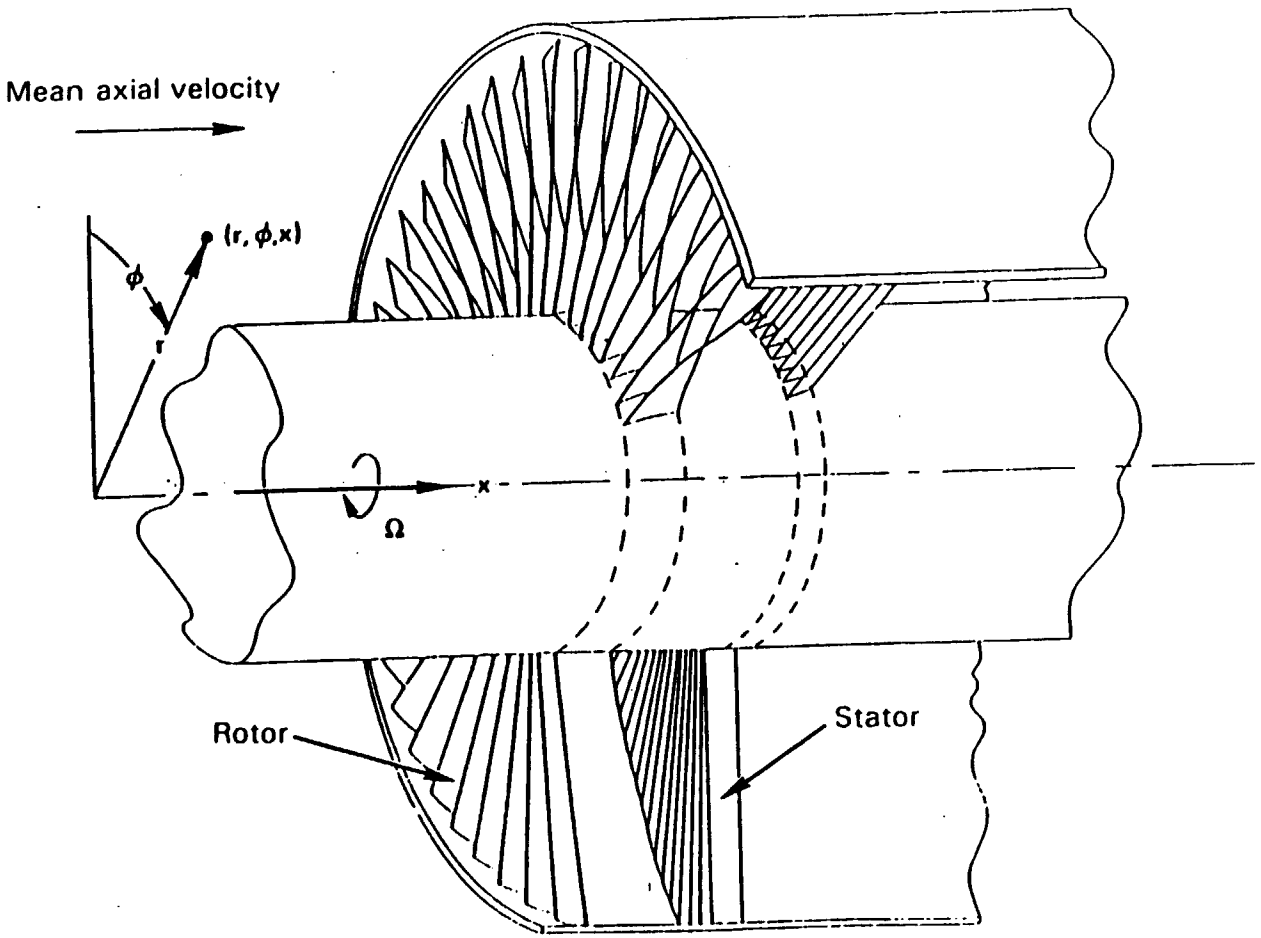

Figure 2. Fan geometry used for study (ref. 11).

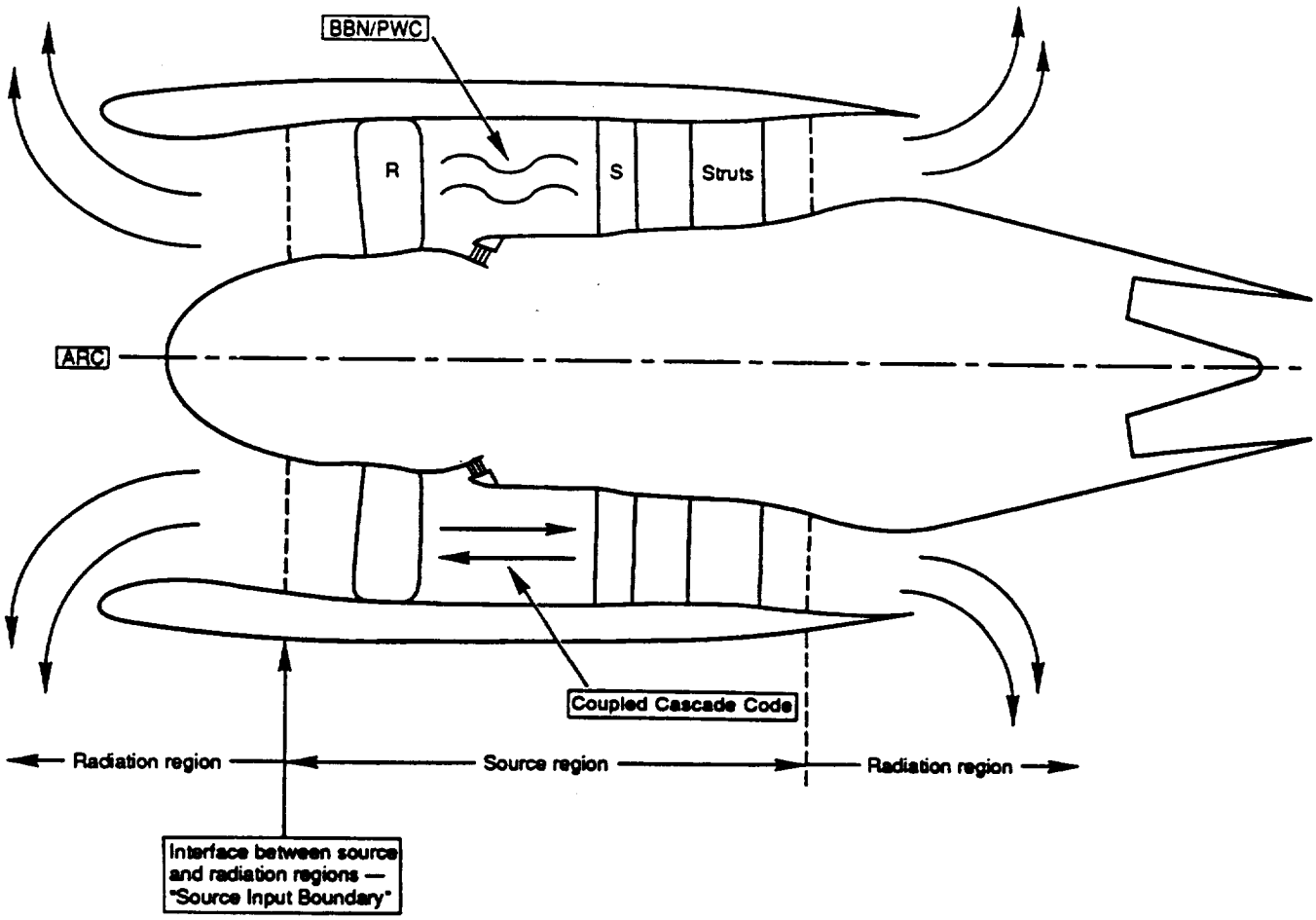

Figure 1. Fan noise design/prediction system (ref. 2).

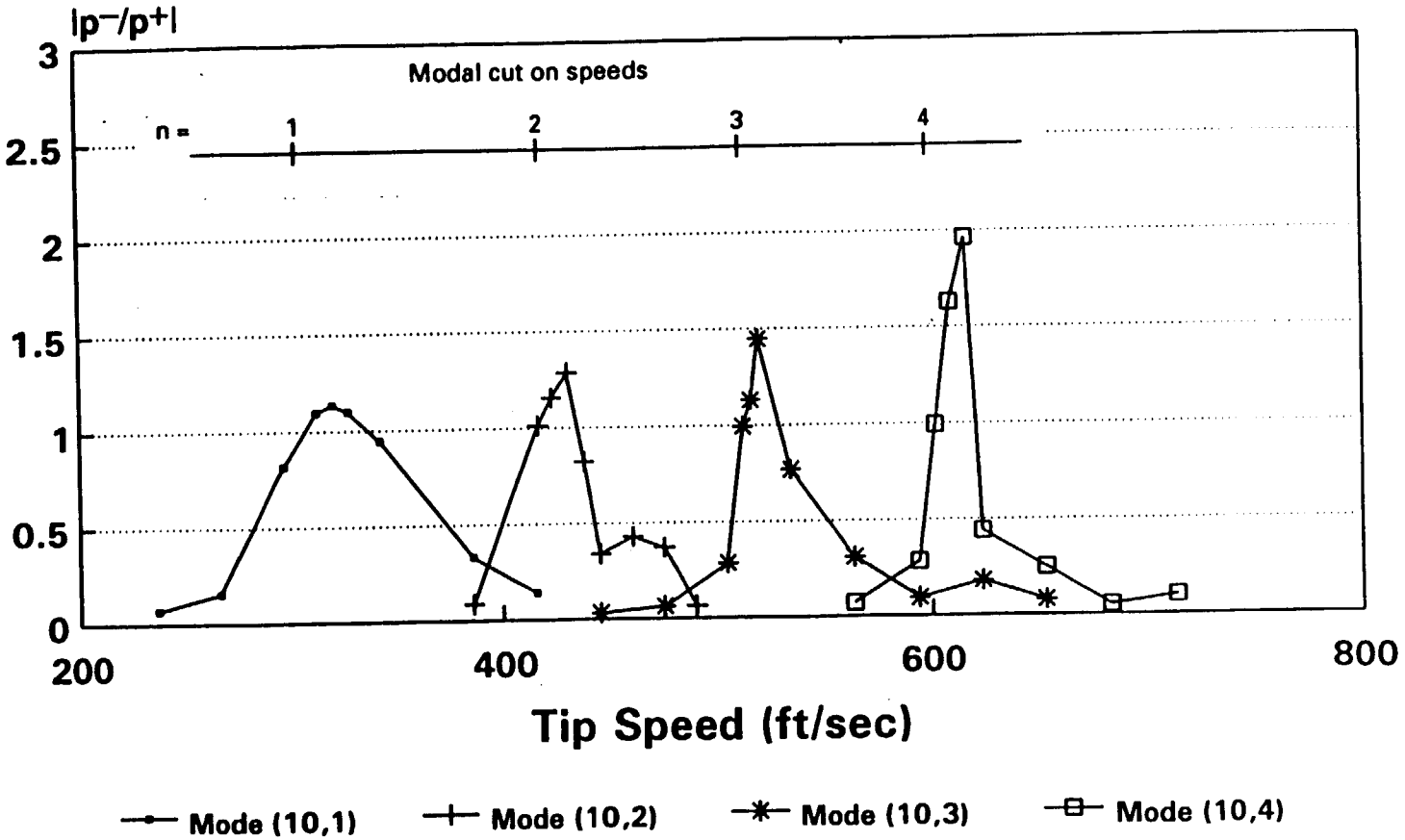

Figure 4. Reflection ratios. $m = 10$, $n = 1$ to 4.

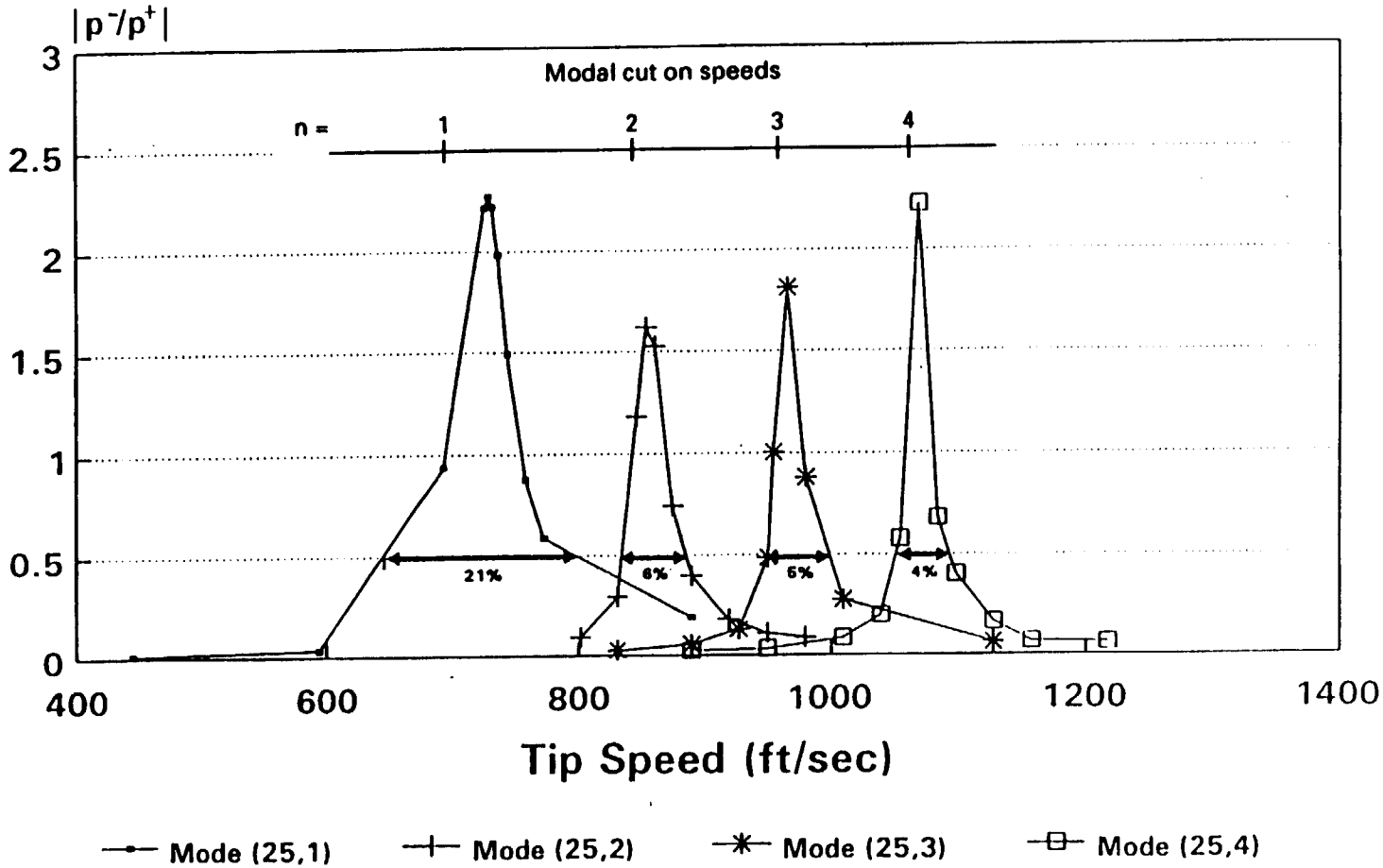

Figure 3. Reflection ratios. $m = 25$, $n = 1$ to 4.

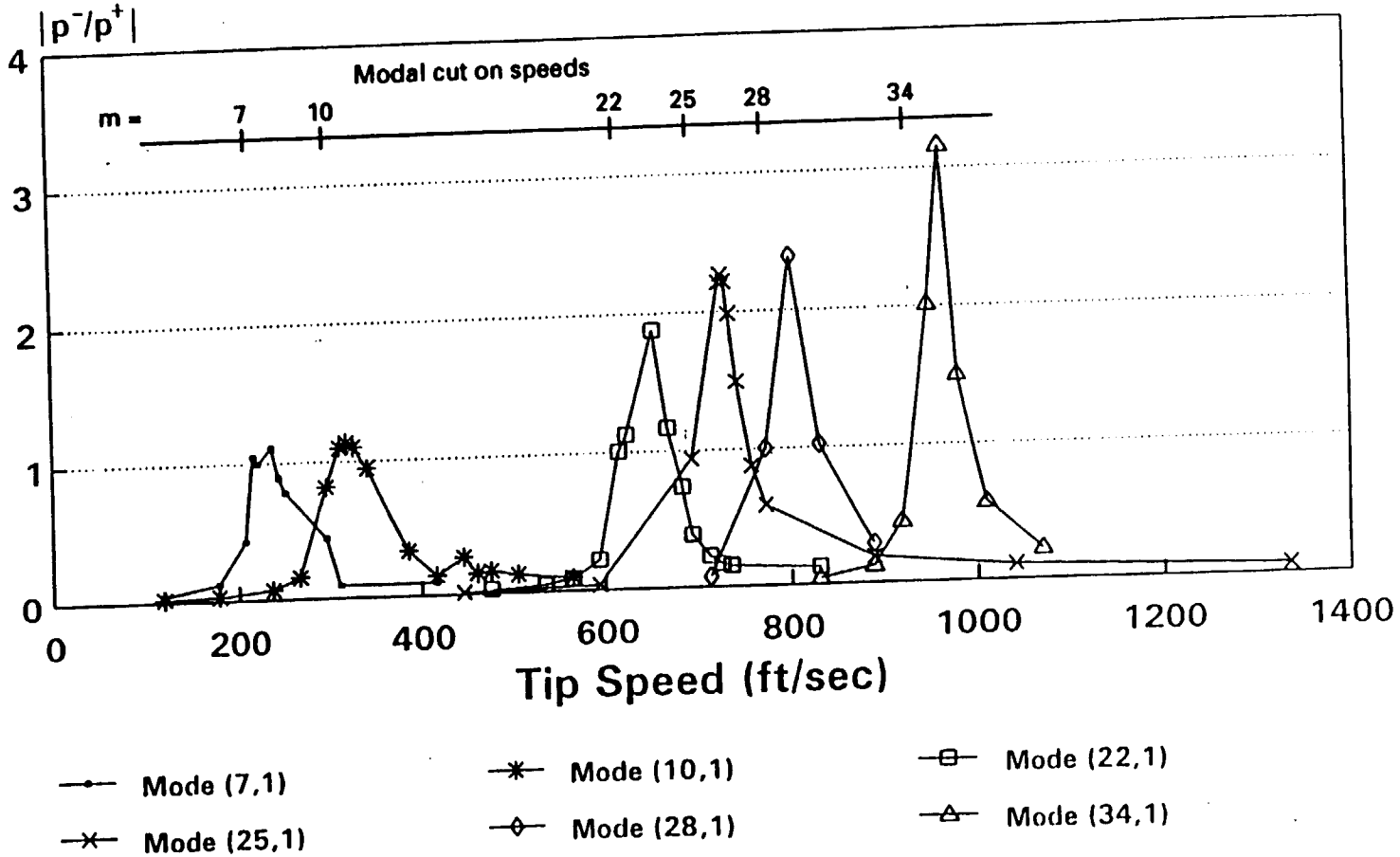

Figure 6. Reflection ratios. m varies, $n = 1$.

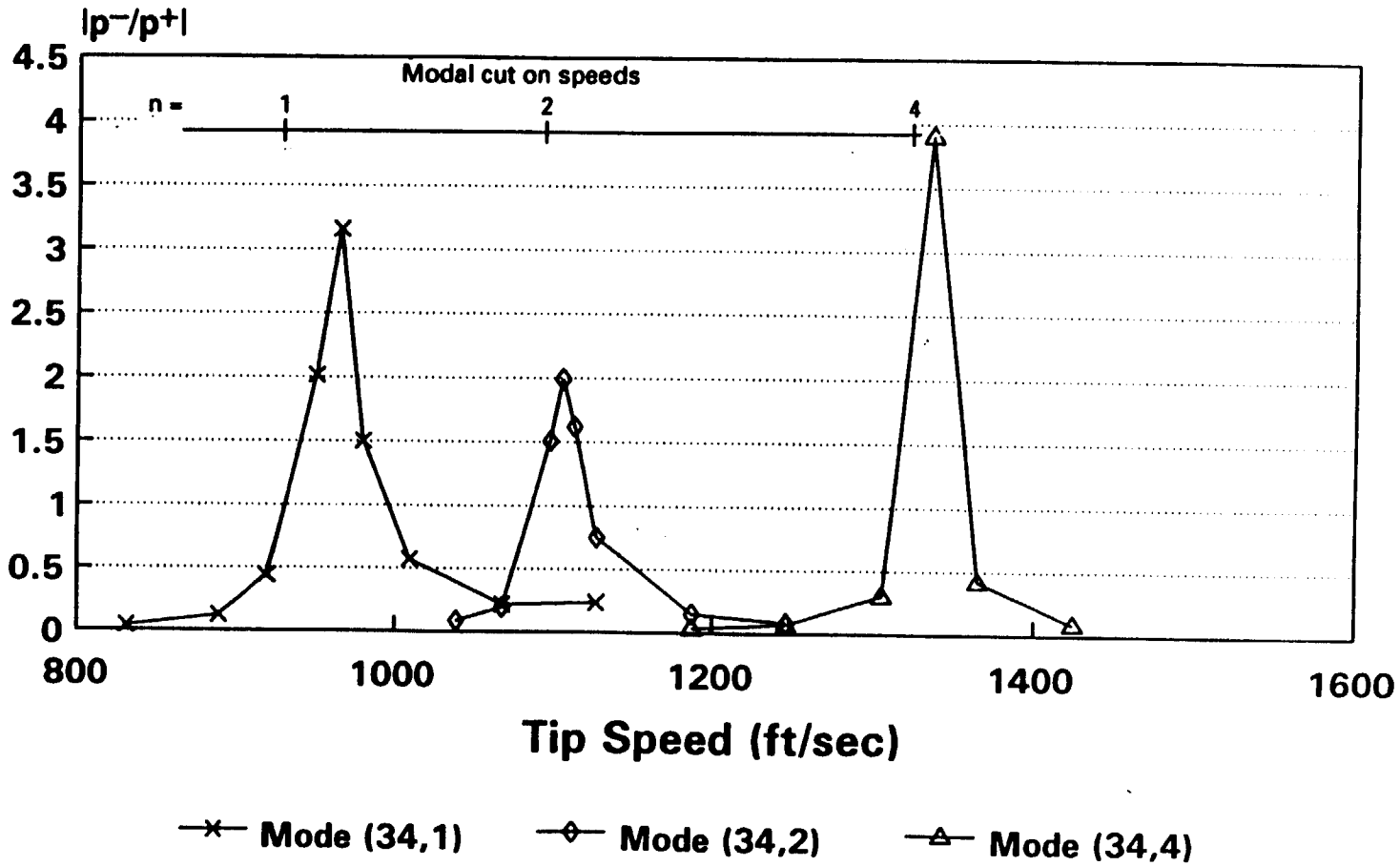

Figure 5. Reflection ratios. $m = 34$, $n = 1, 2,$ and 4.

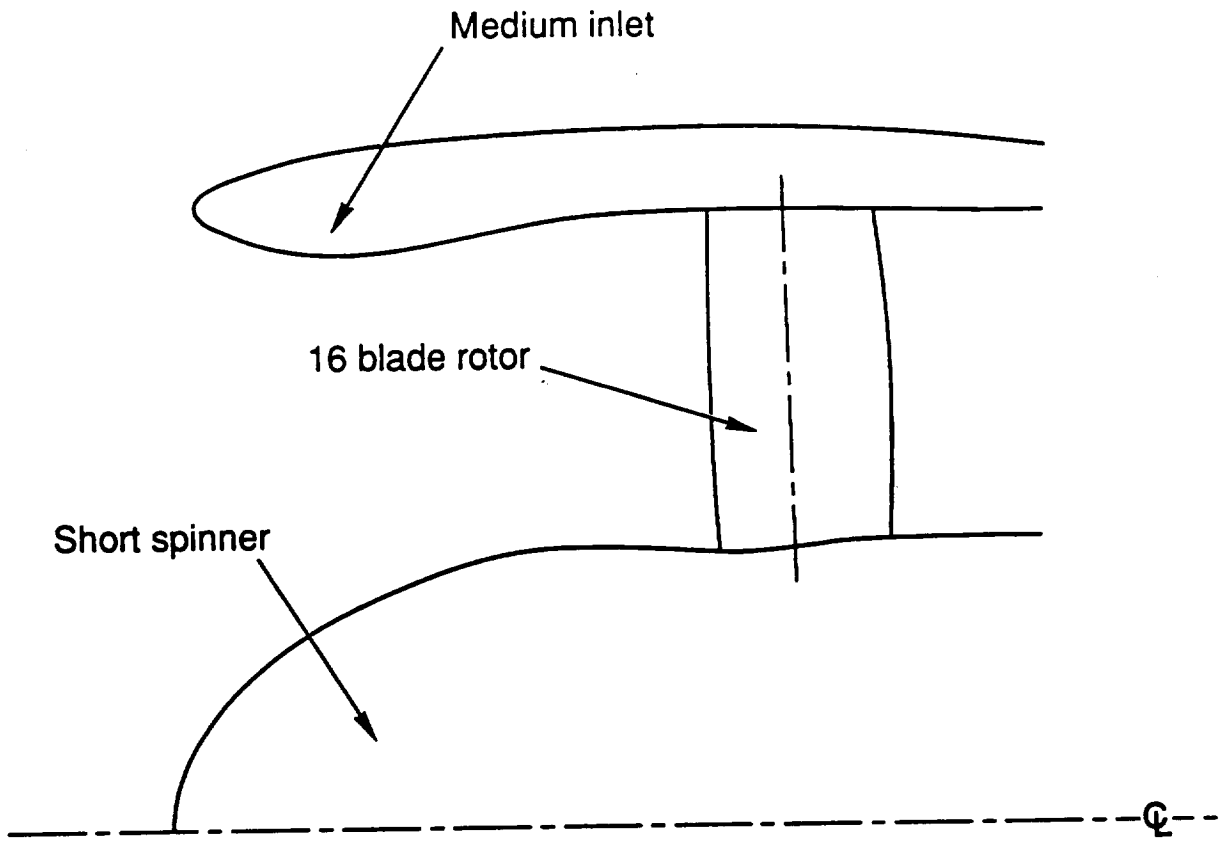

Figure 8. Advanced ducted propeller inlet configuration (ref. 19).

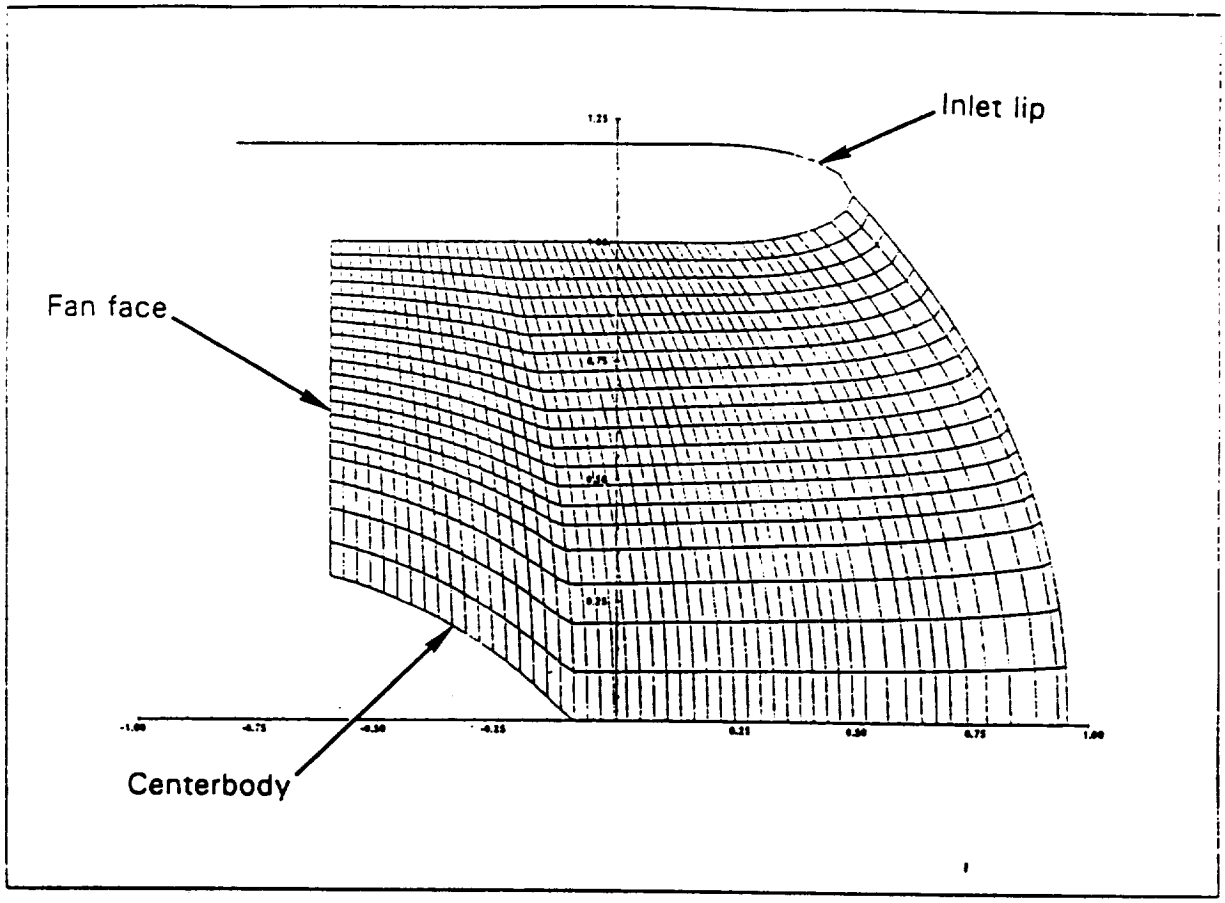

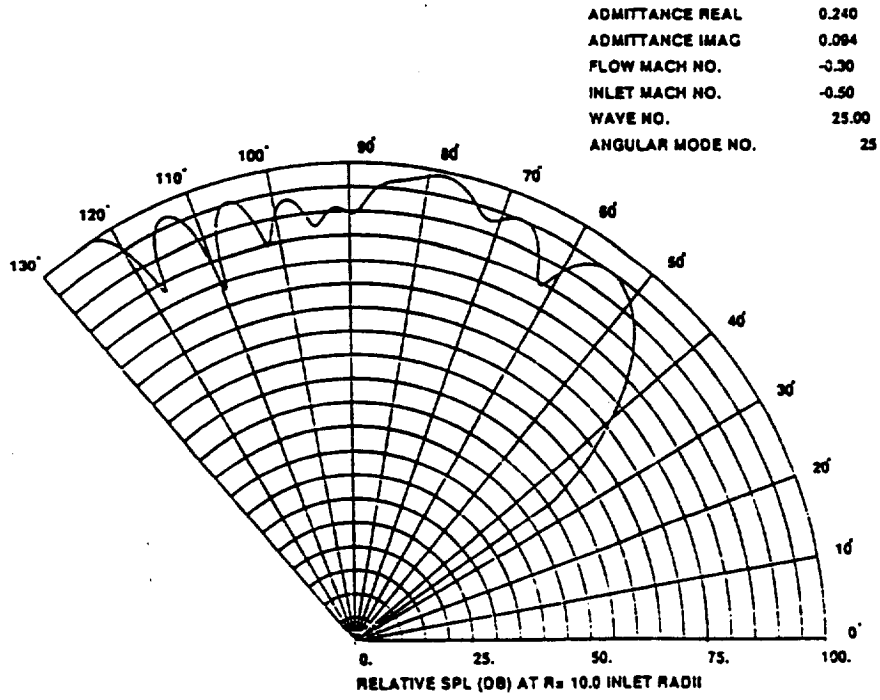

POLAR SPL DIRECTIVITY

Figure 7. Typical PostScript plots. Finite element mesh within the inlet (nomenclature added) and polar SPL directivity.

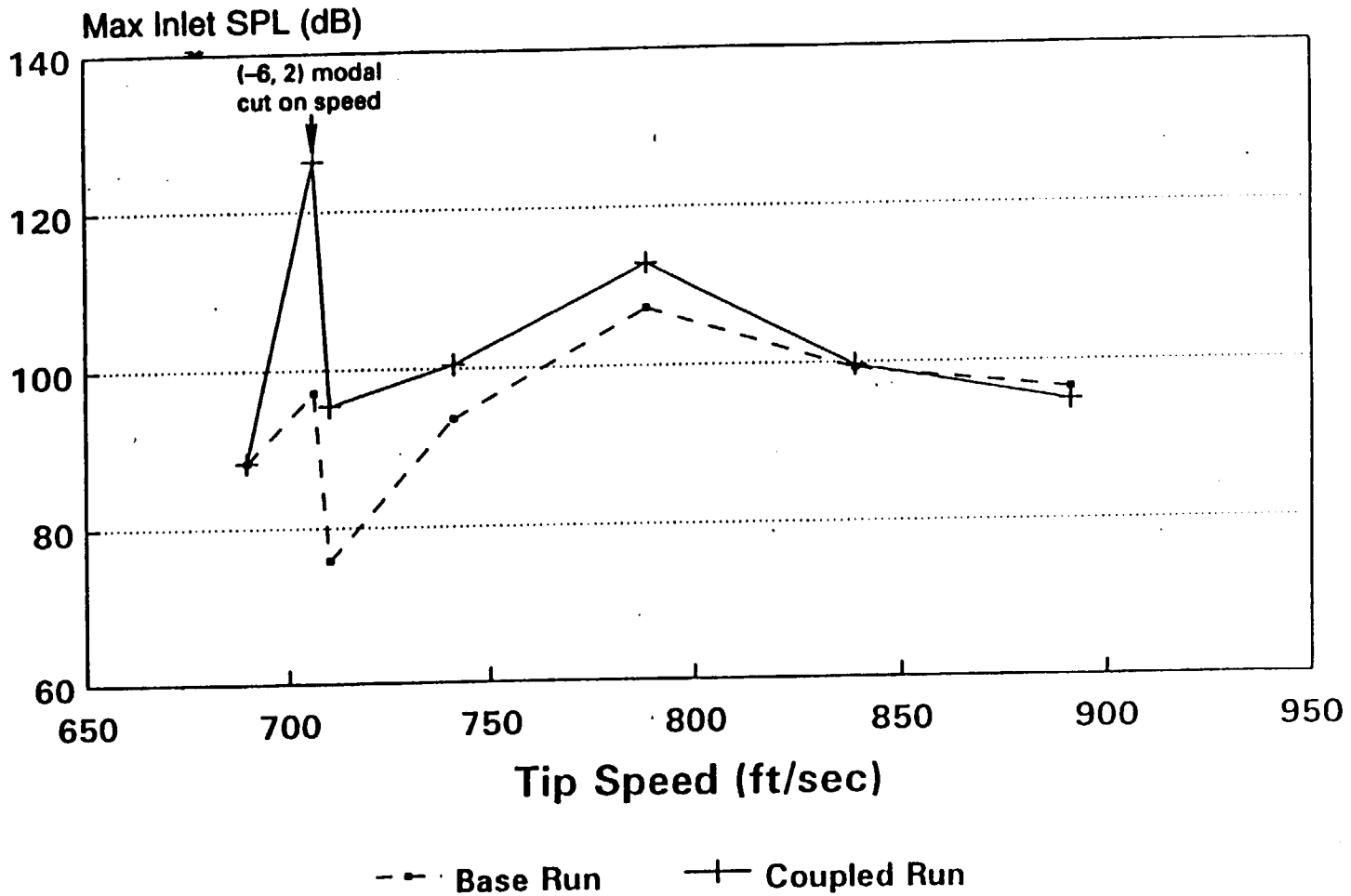

Figure 10. Comparison for ARC runs. Sound Pressure Level at 10 inlet radii for $m = -6$.

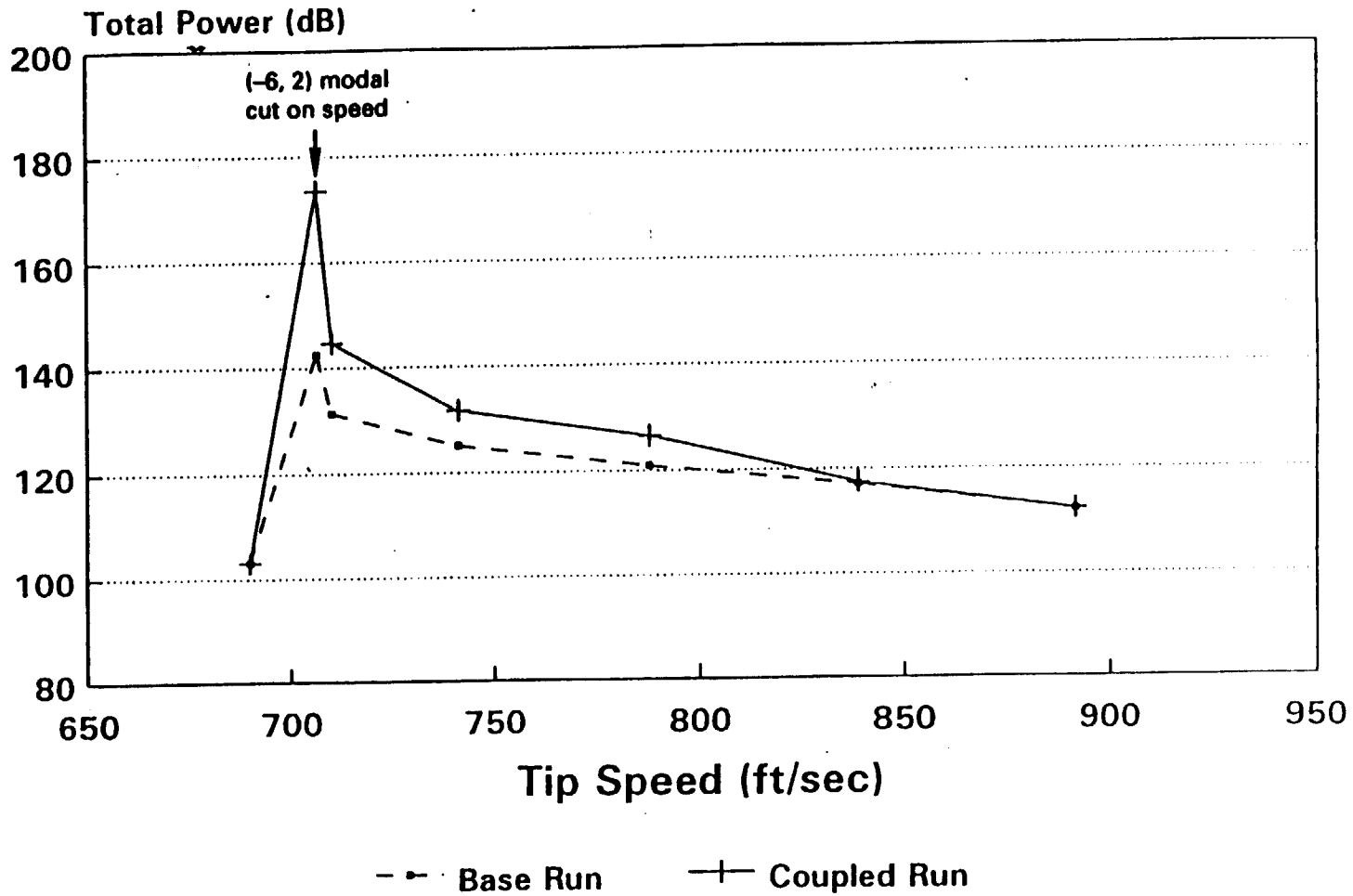

Figure 9. Comparison of BBN/PWC runs. Total upstream power for $m = -6$.

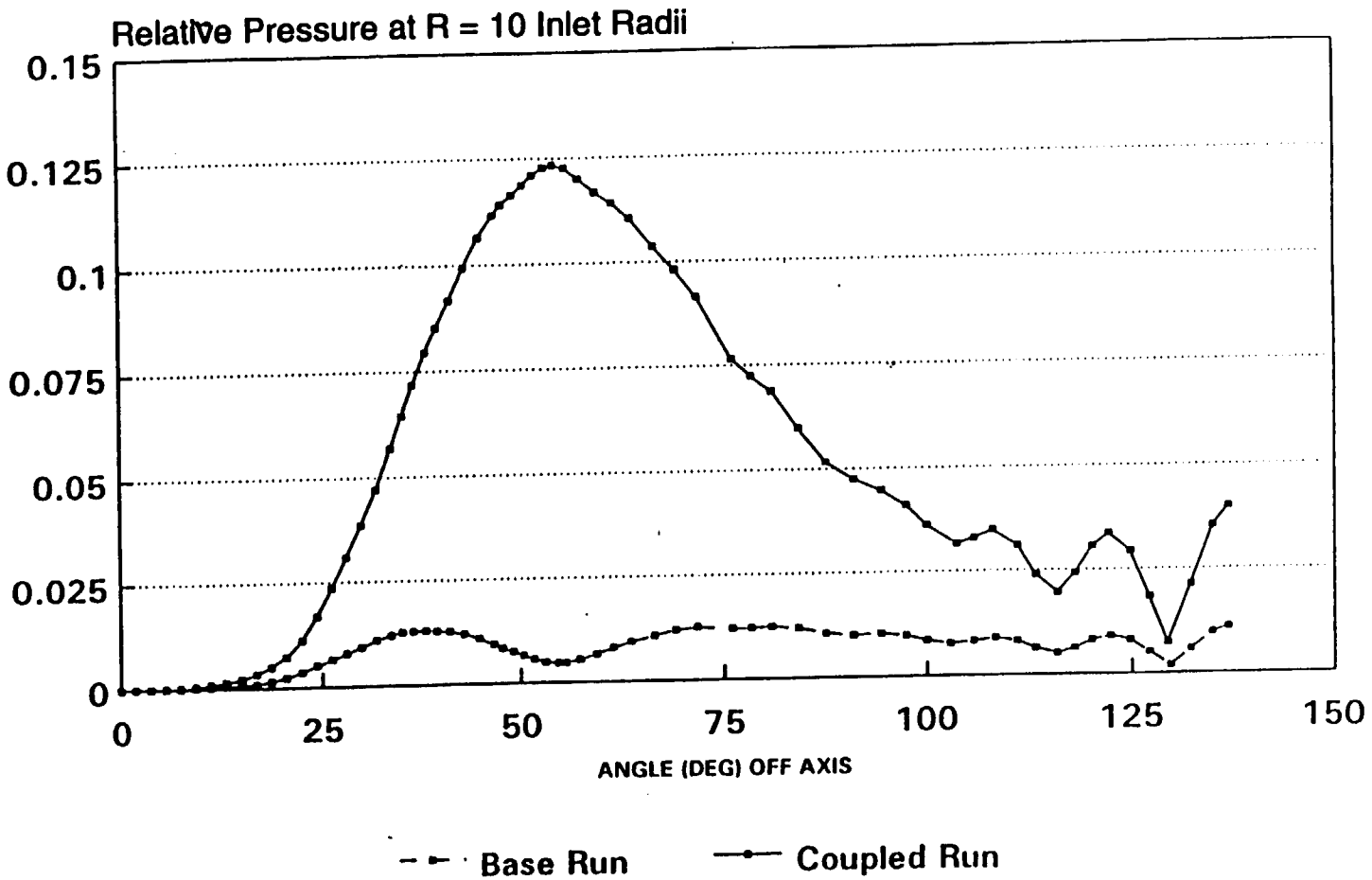

Figure 12. Pressure directivity for $V_T = 710$ ft/sec. Pressure nondimensionialized relative to $\rho_\infty c_\infty^2 \times 10^{-4}$ (19.74×10^{-4} psi).

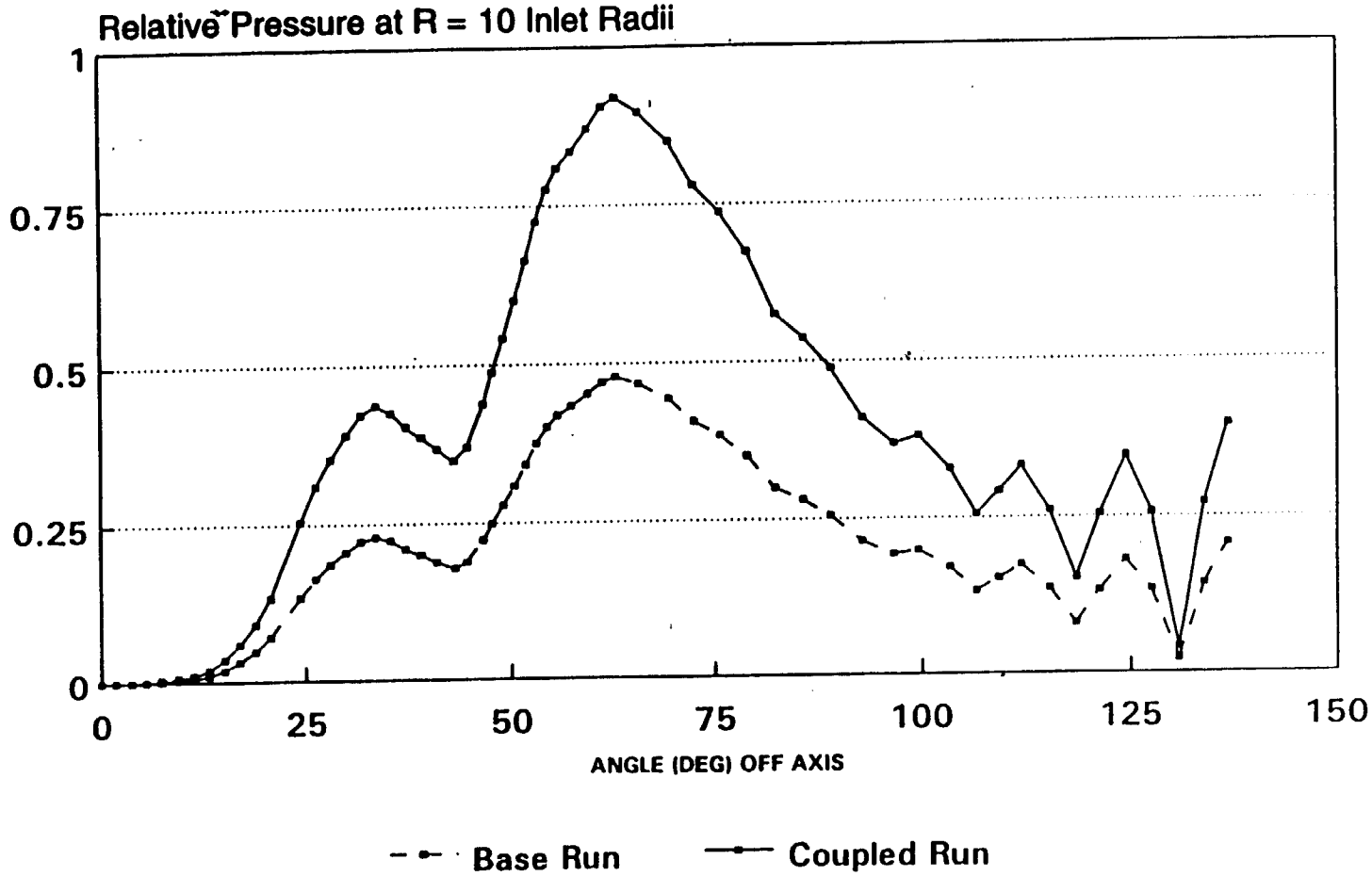

Figure 11. Pressure directivity for $V_T = 788$ ft/sec. Pressure nondimensionialized relative to $\rho_\infty c_\infty^2 \times 10^{-4}$ (19.74×10^{-4} psi).

NASA National Aeronautics and Space Administration

Report Documentation Page

1. Report No.	2. Government Accession No.	3. Recipient's Catalog No.

4. Title and Subtitle	5. Report Date
Fan Noise Prediction System Development: Source/Radiation Field Coupling and Workstation Conversion for the Acoustic Radiation Code	April 1993
	6. Performing Organization Code

7. Author(s)	8. Performing Organization Report No.
H. D. Meyer	None
	10. Work Unit No. PWA-6538-1

9. Performance Organization Name and Address	11. Contract or Grant No.
Hamilton Standard Division United Technologies Corporation One Hamilton Road Windsor Locks, Connecticut 06096	NAS3-25952 (Task 10)
	13. Type of Report and Period Covered
12. Sponsoring Agency Name and Address	Informal Report
NASA-Lewis Research Center 21000 Brookpark Road Cleveland, Ohio 44135	14. Sponsoring Agency Code

15. Supplementary Notes

NASA Task Manager, Dennis Huff, NASA Lewis Research Center
Cleveland, Ohio 44135

16. Abstract

The Acoustic Radiation Code (ARC) is a finite element program used on the IBM® mainframe to predict far-field acoustic radiation from a turbofan engine inlet. In this report, requirements for developers of internal aerodynamic codes regarding use of their program output as input for the ARC are discussed. More specifically, the particular input needed from the Bolt, Beranek and Newman/Pratt and Whitney (turbofan source noise generation) Code (BBN/PWC) is described. In a separate analysis, a method of coupling the source and radiation models, that recognizes waves crossing the interface in both directions, has been derived. A preliminary version of the coupled code has been developed and used for initial evaluation of coupling issues. Results thus far have shown that reflection from the inlet is sufficient to indicate that full coupling of the source and radiation fields is needed for accurate noise predictions. Also, for this contract, the ARC has been modified for use on the Sun® and Silicon Graphics Iris® UNIX® workstations. Changes and additions involved in this effort are described in an appendix.

17. Key Words (Suggested by Author(s))	18. Distribution Statement
Noise, Fan, Acoustics, Radiation, Acoustic Reflection, Acoustic Coupling	

19. Security Classif. (of this report)	20. Security Classif. (of this page)	21. No. of pages	22. Price
Unclassified	Unclassified	45	

NASA FORM 1626 OCT 86